Engineering Structures 348 (2026) 121807

Contents lists available at ScienceDirect

Engineering Structures

journal homepage: www.elsevier.com/locate/engstruct

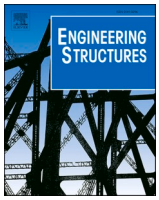

Seismic retrofitting of hollow brick partitions using low-cost self-expanding foam

Gennaro Magliulo [a,b,*], Danilo D'Angela [a], Andrea Prota [a]

[a] University of Naples Federico II, via Claudio 21, Napoli 80125, Italy
[b] Construction Technologies Institute (Naples), National Research Council of Italy, viale Lombardia 49, San Giuliano Milanese, Milan 20098, Italy

ARTICLE INFO

Keywords:
Seismic performance
Nonstructural
Partitions
Retrofitting
Dynamic identification

ABSTRACT

The study was aimed at assessing the effectiveness of a rapid and low-cost solution for seismic retrofitting of hollow brick partitions, in the context of both existing and new buildings. The retrofitting solution, consisting in a detailing variant, was implemented by providing lateral and superior thin slots between partition panels and surroundings, injected by self-expanding polyurethane foam. Shake table tests were carried out according to the international shake table protocol AC156. Both dynamic identification and seismic performance tests were carried out up to peak table accelerations representative of high seismic hazard conditions. Dynamic properties, hysteretic behavior, and capacity measures were associated with physical damage conditions and conventional damage states. A safety assessment was carried out by comparing experimental capacities and code demand measures, considering low to high seismicity sites (in Italy) and both importance class II and IV buildings. The retrofitted partition response and performance was compared to the one associated with non-retrofitted conditions, and it was confirmed that the developed retrofitting solution potentially reduces the seismic vulnerability of hollow brick partition panels. A simplified initial cost and seismic loss/repair analysis referred to a realistic building/apartment scenario finally proved the potential effectiveness of the retrofitting intervention.

1. Introduction

Damage of nonstructural elements (NEs) should be prevented in case of frequent earthquake events, especially for critical facilities [1,2]; as an example, hospital facilities must provide timely critical healthcare services to communities during emergencies [3]. Therefore, the response of NEs should be accounted for when seismic risk of buildings and facilities is assessed.

Among NEs, infills and partitions within frame structures are typically highly vulnerable to low seismic actions [4] since (a) they are typically not seismically designed or they are conceived to remain undamaged under frequent seismic actions [5]. Damage to these elements might be critical in terms of facility functioning [6,7], economic losses [8,9], and casualties, as well as they can interact with structural members and significantly influence the seismic behavior of the building [10,11].

Literature studies on infills and partitions mostly focused on following research objectives: (1) post-event seismic damage assessment [12–14], (2) losses and repair costs assessment [15,16], (3) dynamic identification and seismic assessment through experimental methods [17–19], (4) numerical modeling and analysis [20–24], and (5) improving seismic performance by development of innovative solutions [25–27]. In terms of behavior features, literature studies often focused on (a) influence on global building response [28–30], (b) in-plane/out-of-plane response and interaction [31–33] and (c) local phenomena and failure modes [34,35].

Hollow brick partitions are widely used in Southern Europe and Mediterranean countries for both infills and internal partitions [36]. This is often due to their properties of fire resistance and thermal/-acoustic insulation, along with good interaction with cables and building fixtures, such as (semi-)permanent building technical/functional elements (e.g., secondary support systems or fixed furniture). However, these systems typically exhibit critical behavior under seismic actions in terms of in-plane deformation capacities and out-of-plane acceleration sensitivity. Inadequate partition to structure interface connections typically represent the most critical weakness associated with these systems [14,37], especially for existing buildings but even for new ones.

Among the potential technical solutions developed in the literature and implemented in the practice, disconnecting partition panels from the lateral and superior boundaries is an adopted practice in seismic-

* Corresponding author at: University of Naples Federico II, via Claudio 21, Napoli 80125, Italy.
E-mail addresses: gmagliul@unina.it (G. Magliulo), danilo.dangela@unina.it (D. D'Angela), aprota@unina.it (A. Prota).

https://doi.org/10.1016/j.engstruct.2025.121807
Received 13 May 2025; Received in revised form 31 October 2025; Accepted 14 November 2025

prone countries [38–41]. In some cases, sliding joints were implemented within the masonry panel to improve the seismic performance. Milanesi et al. [42] developed a masonry infill system provided with sliding joints within the panel and deformable joints at the interface with the frame; the system was found to be promising considering both in-plane and out-of-plane resistances. Huang et al. [43] tested a prefabricated wall panel system provided with an opening that integrates sliding joints, and it was found to be highly deformable and dissipative. Both systems were meant to be applied with regard to infill construction rather than as a retrofitting technique.

For masonry partitions, effective gaps between panels and frame members might range within 20–80 mm width at the interface with columns and are about 25 mm at the interface with beam/slab [39]. These gaps are usually incorporated during the construction phase rather than introduced as part of retrofitting interventions, and the approach presents several limitations [40]. (1) The out-of-plane seismic vulnerability of the panels can be critical, as they behave as cantilevers and might significantly amplify the accelerations. Consequently, technical solutions must provide out-of-plane protection while preventing in-plane structural interaction; however, these solutions are often costly and difficult to implement. (2) The required gap widths are relatively large, and, whereas this may be feasible during new construction, implementing such gaps as part of a retrofit is generally invasive, time-consuming, and expensive. (3) Gaps may compromise performance in terms of thermal insulation, fire safety, and other safety and comfort requirements. (4) Finishing the gaps is often challenging, and the treatment can be prone to degradation from low-intensity vibrations, leading to the need for frequent cosmetic repairs. Therefore, even though the idea of disconnecting partition and infill masonry panels to the structure has potential, the existing solutions are not effective and further effort is needed, especially for retrofitting (and not construction) purposes.

In this paper, an effective and rapid and low-cost solution, consisting in a detailing variant, is developed to improve the seismic performance of hollow brick partitions, with a focus on the partition to structure interfaces. In particular, the concept of panel to structure gap is enhanced by (a) significantly reducing its width and (b) injecting self-expanding polyurethane foam. This approach enables a peculiar interaction between structure and partitions panels, improving seismic performance while being minimally invasive, rapid to apply, and cost-effective. No other studies, to the authors' knowledge, investigated similar detailing solutions [39,40], and, whereas polyurethane injection has been proven to be effective for seismic improvement of geotechnical systems [44,45], no applications tested the effectiveness of the above-mentioned injections for mitigating the seismic risks associated with infills and partitions. The retrofitted specimens are tested on shake table; the effectiveness of the retrofitting solution is quantified and also referred to safety checks. Finally, cost and effectiveness analyses are carried out.

2. Methodology

The test setup consists of a shake table, a steel testing frame (main frame), a secondary frame system, and three specimens (retrofitted hollow brick partitions), as depicted in Fig. 1. The three specimens included a wide panel and two identical narrow panels. The tested specimens are referred to as retrofitted (R) specimens, and the reference for the non-retrofitted (NR) specimens is [46]

2.1. Shake table and main frame

The tests aimed to reproduce seismic demands consistent with a structural cell of a code-conforming building in which the partitions are meant to be constructed. The seismic input was assigned to the shake table [46] that transferred the actions to a main test frame, fixed to the table. A secondary frame provided fixed to a base concrete slab was rigidly fastened to both shake table and main frame top, and this secondary frame housed three partition panels.

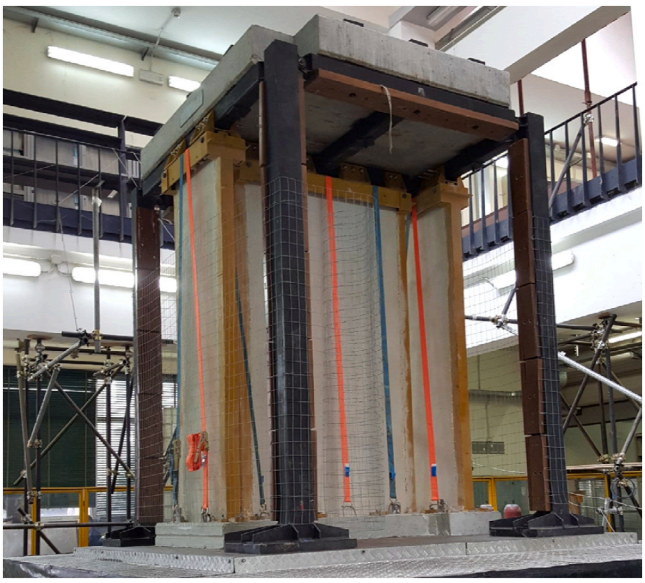

Fig. 1. Global view of the test setup prior to the tests.

The main frame was designed to comply with a code-conforming generic frame building, in terms of applied masses on the frame top and realistic stiffness earthquake, representing a frequent earthquake associated with damage limitation limit state (DLS). The test frame was designed to exhibit a 0.5 % interstory drift ratio (IDR) for an earthquake characterized by spectral response acceleration at short periods (S_{DS}) equal to 0.60 g (peak ground acceleration (PGA) equal to 0.24 g [37]).

2.2. Specimens and secondary frame

The specimens were prepared following two steps: (1) building the traditional hollow brick partition panels and (2) implementing the retrofitting interventions. The specimens consist of three partition panels, i.e., a (longitudinal) wide panel having a 150 cm width and two (perpendicular) small panels having a 80 cm width; the partition panels were 2.6 m high. The dimension of the partition panels was determined by making a compromise between (a) a sufficiently large width to account for realistic installations (e.g., larger than 1 m) and sufficiently narrow to be able to investigate damage states (DSs) up to severe damage conditions. Further details can be found in [46,48–50].

The traditional hollow brick partitions were made of 250 × 250 × 80 mm hollow bricks, jointed and plastered with mortar and with staggered vertical joints. The bricks are compliant with UNI EN 771–1 [51], with a hollow area ranging in 55 % - 70 % of brick cross-sectional area. The volumetric density of the blocks is 605 kg/m^3 , and the mass per surface unit of the brick-mortar system is 60 kg/m^2. The characteristic compressive strength of the blocks exceeds 5.0 N/mm^2 in the longitudinal direction of the hollows and 1.5 N/mm^2 in the perpendicular direction. The base of the partition panels was connected to the shake table by means of an "I" shaped RC slab. The partition panels were connected to the main steel frame through a secondary steel frame. The secondary frame was designed to reproduce, in a realistic manner, the interaction between the partition panels and representative boundary conditions. Moreover, the secondary frame was defined to be so flexible to not structurally interact with the response of the tested panels, as is quantified in the following.

The columns of the secondary frame had "C" shape section with 90 mm flange width, 90 mm web depth, and 5 mm (10 mm) flange (web) thickness, and were connected to the upper transverse beam through a pin connection so to have a hinge connection in the partition

panel's direction and a rigid connection in the out-of-plane direction. The bricks were alternatively clamped within the "C" profiles, whereas the alternate panel to vertical secondary frame stud gaps were filled with mortar (Fig. 2.b) to reproduce the presence of perpendicular panels at the adjacency of the tested panel [46], as this condition is frequently implemented in real installations of hollow brick partitions.

The stiffness contribution of the secondary frame columns was more than an order of magnitude lower than the one associated with the partition panels. In particular, the flexural stiffness of the single "C" profiles along in-plane and out-of-plane (panel's) direction was computed as reported in Eqs. (1) and (2), respectively, referring to $K_{1,IP}$ and $K_{1,OOP}$, according to the previously defined implemented connection details. E, I_W, I_S, and h define Young's modulus, weak and strong axis moment of inertia, and column height, respectively.

$$K_{1,IP} = \frac{3EI_W}{h^3} \quad (1)$$

$$K_{1,OOP} = \frac{12EI_S}{h^3} \quad (2)$$

The total lateral stiffness contribution of the secondary frame was calculated as the sum of all relevant profile flexural stiffnesses along X and Y directions ($K_{SF,X}$ and $K_{SF,Y}$). The lateral stiffness of the partition panels was computed as reported in Eq. (3) for both narrow and wide panels. $K_{PP,F}$ and $K_{PP,H}$ are flexural and shear stiffness, respectively: $K_{PP,F}$ computed as it was done for the secondary frame column profile and $K_{PP,H}$ according to Eq. (4), where G and A are shear modulus and cross-section area, respectively. Narrow (wide) in-plane and out-of-plane panel lateral stiffness are defined as $K_{PP,N,IP}$ and $K_{PP,N,OOP}$ ($K_{PP,W,IP}$ and $K_{PP,W,OOP}$), respectively.

$$K_{PP} = \frac{1}{\frac{1}{K_{PP,F}} + \frac{1}{K_{PP,H}}} \quad (3)$$

$$K_{PP,H} = \frac{GA}{h} \quad (4)$$

The stiffness values associated with main frame, partition panels, and secondary frame are reported in Table 1. Total setup stiffness (K_{TOT}) was computed by summing all member stiffness and was reported in Table 2, together with partition panels and secondary frame stiffnesses divided by K_{TOT}. Along X and Y direction, the influence of partition panels on total setup stiffness is equal to 92 % and 94 %, respectively, and the contribution of the secondary system corresponds to 2 %, confirming that the stiffness of the secondary frame does not interfere with the partition in resisting to the horizontal actions.

Table 1
Stiffness values associated with main frame, partition panels, and secondary frame, along in-plane (IP), out-of-plane (OOP), X, and Y directions.

Main frame	Partition panels				Secondary frame			
K_{FX} (K_{FY})	$K_{PP,N,IP}$	$K_{PP,N,OOP}$	$K_{PP,W,IP}$	$K_{PP,W,OOP}$	$K_{1,IP}$	$K_{1,OOP}$	$K_{SF,X}$	$K_{SF,Y}$
kN/m	kN/m	kN/m	kN/m	kN/m	kN/m	kN/m	kN/m	kN/m
3050	22400	227	66500	425	46.9	327	841	1400

Table 2
Stiffness associated with total setup (K_{TOT}) and partition panel stiffness (K_{PP}) and secondary frame stiffness (K_{SF}) divided by total frame (K_{TOT}) along X and Y direction.

$K_{TOT,X}$	$K_{TOT,Y}$	$K_{PP,X}/K_{TOT,X}$	$K_{PP,Y}/K_{TOT,Y}$	$K_{SF,X}/K_{TOT,X}$	$K_{SF,Y}/K_{TOT,Y}$
kN/m	kN/m	[-]	[-]	[-]	[-]
49200	71450	0.92	0.94	0.02	0.02

2.3. Retrofitting

The retrofitting intervention was implemented after the construction of the traditional hollow brick partition panels. Firstly, the lateral ends of the partitions were fully disconnected through a cut from the secondary frame columns by implementing a 5 mm width gap corresponding to the panel to frame interface (Fig. 3.a,b). Afterwards, the gap was filled by a low-cost self-expanding polyurethane foam (Fig. 3.c,d). The retrofitting consists in applying self-expanding polyurethane foam packaged in a pressurized can by a specific gun within the above-mentioned 5 mm gap at the interface between the panels and the secondary frame (Fig. 3.c).

The product is made of a mixture of polyurethane prepolymer, specific foaming agents, and special additives, free of chlorofluorocarbons

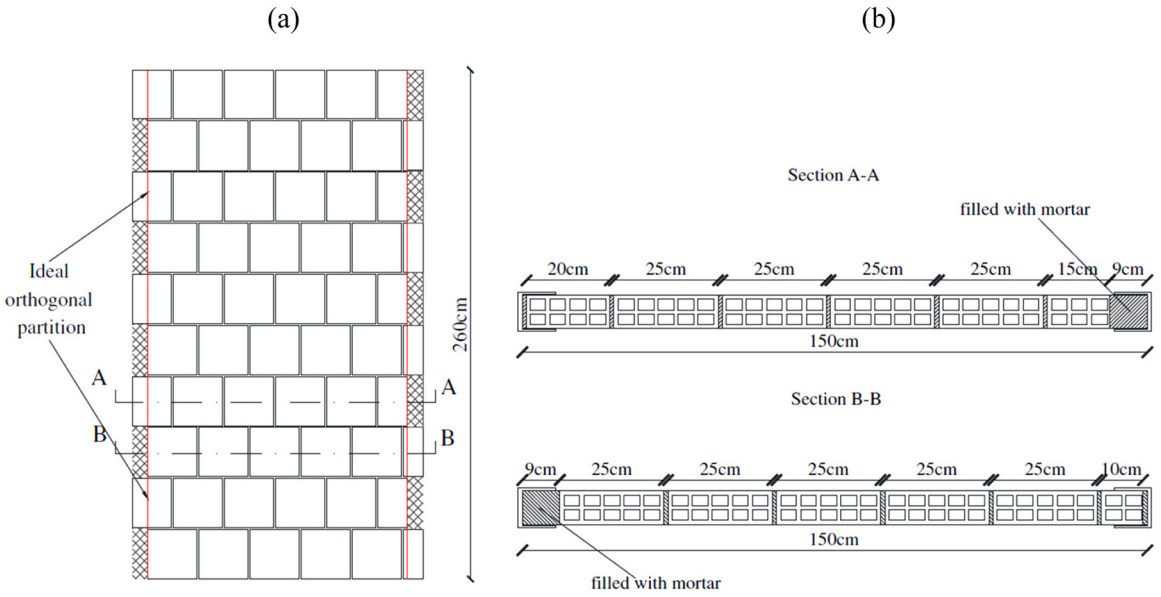

Fig. 2. (a) Lateral view and (b) cross section of the hollow brick partition panel. The alternate panel to vertical secondary frame stud gaps are filled with mortar to reproduce the presence of perpendicular panels at the adjacency of the tested panel [46].

Fig. 3. Implementation of the retrofitting system: (a) initiation of secondary frame to partition panel gap, (b) secondary frame to partition panel gap, (c) foam filling of secondary frame to partition panel gap, (d) fully foam filled secondary frame to partition panel gap.

and not harmful to the ozone layer. The foam expands in volume and hardens quickly after extrusion due to the humidity, and it forms a stable closed-cell structure with excellent mechanical properties and high thermal and acoustic insulation properties. This foam, and similar ones, are produced by several construction material manufacturers and is typically used for filling, sealing, and isolating voids and discontinuities of multiple construction details in buildings and other engineering systems, often to also confer thermo-acoustic isolation layers. The technical and performance parameters provided by the manufacturer are reported in Table 3.

The proposed retrofitting solution is primarily intended for existing buildings but can also be implemented during new construction (easier implementation). For existing buildings, a 5 mm slot should be created (by cut) at the interface between the partition panel and its lateral and upper boundaries and injected with foam; it can be applied for both adjoin columns or perpendicular partitions. In new construction, the slot can be formed directly by interrupting the brickwork at these same interfaces, at connections with columns or perpendicular partition panels.

Table 3
Technical sheet of the polyurethane foam.

Application data	
Application temperature	from + 5°C to + 30°C
Ideal storage temperature:	from + 20°C to + 25°C
Flammability class (DIN 4102)	B3
Performance data	
Dust-free time (at +23°C and 50 % R.H.) [min]	5–10
Operating temperature	from −40° to 90°
Minimum time for foam cutting (Ø 20 mm at +20°C and 60 % R. H.) [min]	25–30
Full curing time [h]	1.5 – 5
Free expansion [L]	45
Compressive strength [N/cm^2]	4.5
Tensile strength [N/cm^2]	7.5
Elongation at break [%]	25
Density [kg/m^3]	17
Shrinkage (after 24 h at +20°C and 60 % R.H.) [%]	1
Water absorption after 24 h (DIN 53428) [%]	1
Thermal conductivity at + 20°C (DIN 52612) [W/m·K]	0.036
Sound insulation (EN 12354–3 or EN ISO 717–1) [dB]	58

2.4. Instrumentation and testing procedure

The response of table and specimens was monitored by accelerometers (Acc.) and laser sensors (Las.), as depicted in Fig. 5 and detailed in the Appendix. The experimental tests were performed through shake table testing. Both dynamic identification tests and seismic performance (incremental) tests were carried out. Dynamic identification tests were carried out via unidirectional excitations to enhance the accuracy of modal parameter estimation by facilitating the separation and clearer interpretation of the vibration modes along each principal direction and minimizing modal coupling, whereas seismic performance evaluation tests were performed under bidirectional loading to realistically reproduce the multidirectional nature of earthquake ground motions and assess the spatial seismic response, including interactions between directions, which are critical for the tested specimens [46].

The experimental tests were carried out according to the AC156 protocol [48], which provides requirements and procedures for seismic qualification and certification of NEs, applicable if the NE fundamental frequency is greater than 1.3 Hz. The protocol is compliant with US codes [52,53] and widely applied in the literature [27,41]. The protocol implicitly accounts for the building-to-building and record-to-record uncertainty, and the strict compliance with the protocol guarantees a high reliability to the tests, allowing to consider the assessment as a qualification procedure.

The seismic input for the seismic performance evaluation is a nonstationary broadband random signal and features an energy content within 1.3 and 33.3 Hz. The bandwidth resolution is one-sixth octave, and the input has 20 s of strong-motion and is compatible with protocol required response spectrum (RRS). The seismic inputs defined and used by Petrone et al. [46] was employed to favor consistent comparisons and to clearly highlight the influence of the retrofitting intervention. In particular, NE installation height (z) to building height (H) ratio (z/H) was assumed unitary to account for the most amplified building response (NE installed on the roof). Fig. 4 shows the time histories and the related pseudo-acceleration spectra corresponding to S_{DS} equal to 1.5 g.

Ten AC156 (AC01-AC10) tests were carried out, from a S_{DS} equal to 0.10 g (AC01) up to 1.00 g (AC10), through step increments of 0.10 g.

Dynamic identification tests were performed prior to and after each performance test to assess the dynamic properties of the specimens

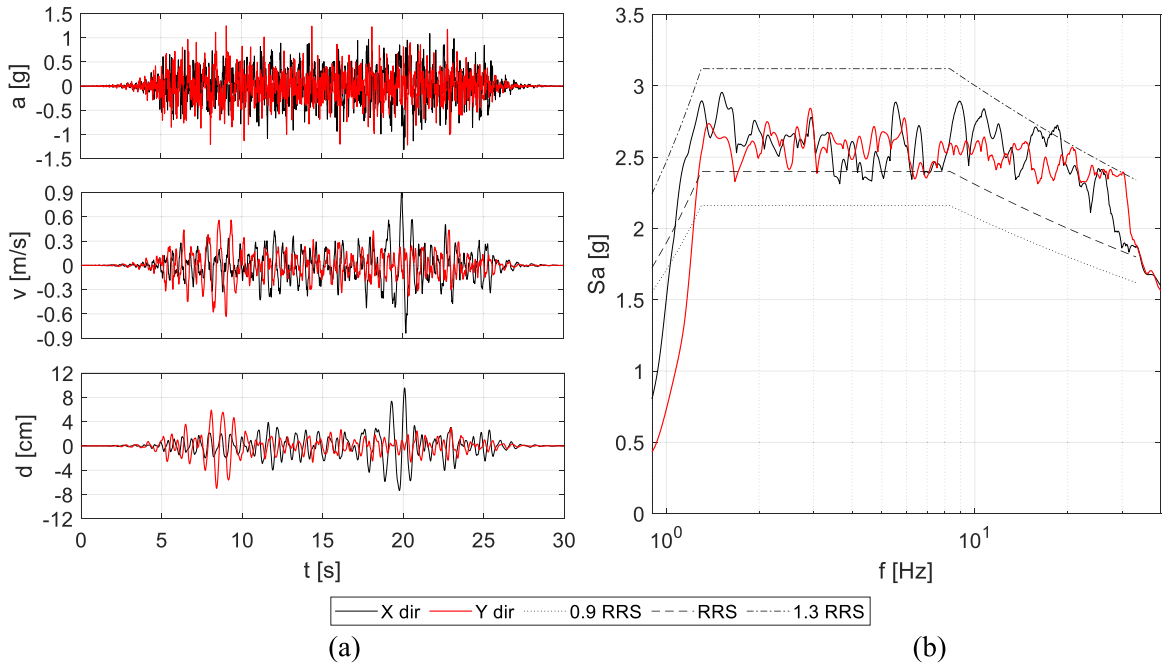

Fig. 4. AC156 protocol signals used for the seismic performance evaluation tests: (a) acceleration (a), velocity (v), and displacement (d) time histories and (b) pseudo-acceleration spectral ordinates (Sa), expressed as a function of elastic frequency (f), along X and Y directions. The signals refer to S_{DS} equal to 1.5 g.

along the incremental tests and associated with the damage process evolution [54]. Low-amplitude random vibration signals (low-intensity noise inputs [46,55]) with peak acceleration not greater than 0.10 g were used to perform the dynamic identification tests along both horizonal directions. Six random (RAN) tests were performed in each direction. RAN1 preceded the tests, RAN2, RAN3, RAN4, RAN 5, and RAN6 followed AC06, AC07, AC08, AC09, and AC10 respectively. Unfortunately, there were some issues related to RAN6, and it was not possible to elaborate the related test results, which would have been informative regarding the dynamic properties associated with the highest intensity damage condition. However, as it is discussed in the following, the conventional damage condition achieved under AC10 was the same observed for previous tests, and the missing elaboration does not affect the significance of the results.

ibration excitations were utilized for the dynamic identification of the sample cabinets, before and during the seismic performance testing steps, using random input signals developed according to FEMA 461 44: they are low-amplitude shakings with root-mean-square limited to 0.05 $\pm$ 0.01 g. Because of the low intensity of these excitations, sliding/rocking of cabinets was not observed

3. Damage states

The technical definition of DSs was based on the definition provided by Taghavi and Miranda [7] and follows the approach implemented in several literature studies [56] (also considering consequences to damage as discussed in post-even surveys [2]). Whereas the consequence assessment and the relevancy to the performance levels (PLs) and limit states (LS) are typically referred to general NEs, the technical definition of the damage conditions, in terms of observed and measured damage, is associated with the specific case study application, compatible with damage of masonry partition walls. The technical definition of the damage exhibited by the partition panel was identified by referring to the potential consequences in terms of relevant PLs and LSs, i.e., operativity limit state (OLS), DLS, and life safety limit state (LSLS).

Infill and partition panels are typically sensitive to relative displacements and accelerations along their in-plane and out-of-plane directions, respectively [57]. Therefore, the specimens can be considered both acceleration- and drift-sensitive. In the case of bi-directional shaking, each specimen was subjected to simultaneous in-plane and out-of-plane excitations, and the seismic demand was transferred to the partition panels through both relative displacements (mainly along in-plane directions) and accelerations (mainly along out-of-plane directions). Typical in-plane seismic damage of infill and partition panels generally consists of corner crushing, sliding shear, diagonal compression, and diagonal cracking, whereas out-of-plane damage typically consists of sliding/expulsion of partition parts (e.g., bricks) and partial or total overturning of the partition panel; the sensitivity of the specific panel to the abovementioned mechanisms strongly depends on the features of the panel. The following DSs were considered: DS0 (absent or negligible damage), DS1 (minor damage), DS2, (moderate damage), and DS3 (major damage).

The technical definition of DSs was reported in detail in the Appendix. DS1 was associated with the potential achievement of OLS, DS2 with DLS, and DS3 with life safety limit state (LSLS). DS0 corresponded to absent or negligible damage, e.g., hairline cracks (width $<$ 0.3 mm). DS1 was technically defined by fine cracks (0.3 mm $\leq$ width $<$ 5 mm) affecting extended areas (e.g., more than 50 % of the partition panel) or by wide cracks (5 mm $\leq$ width $<$ 10 mm) or superficial localized partition spalling in reduced areas (e.g., less than 10 %). DS2 is related to wide cracks (5 mm $\leq$ width $<$ 10 mm) affecting extended areas or severe cracks (10 mm $\leq$ width $<$ 20 mm) or localized partition spalling in reduced areas (e.g., less than 10 %) that do not potentially affect global integrity of the partition panel and safety of occupants. DS3 is associated with severe cracks (10 mm $\leq$ width $<$ 20 mm) in extended areas (e.g., more than 50 %) or severe/extended partition spalling or extremely severe cracks (width $\geq$ 20 mm) or any condition that potentially affects global integrity of the partition panel or safety of occupants.

4. Experimental results

4.1. Damage survey and damage state identification

The wide partition panel is (more) representative of real building applications since the panel sizes are compatible with realistic building installations. Regarding the wide partition panel, no visible damage of

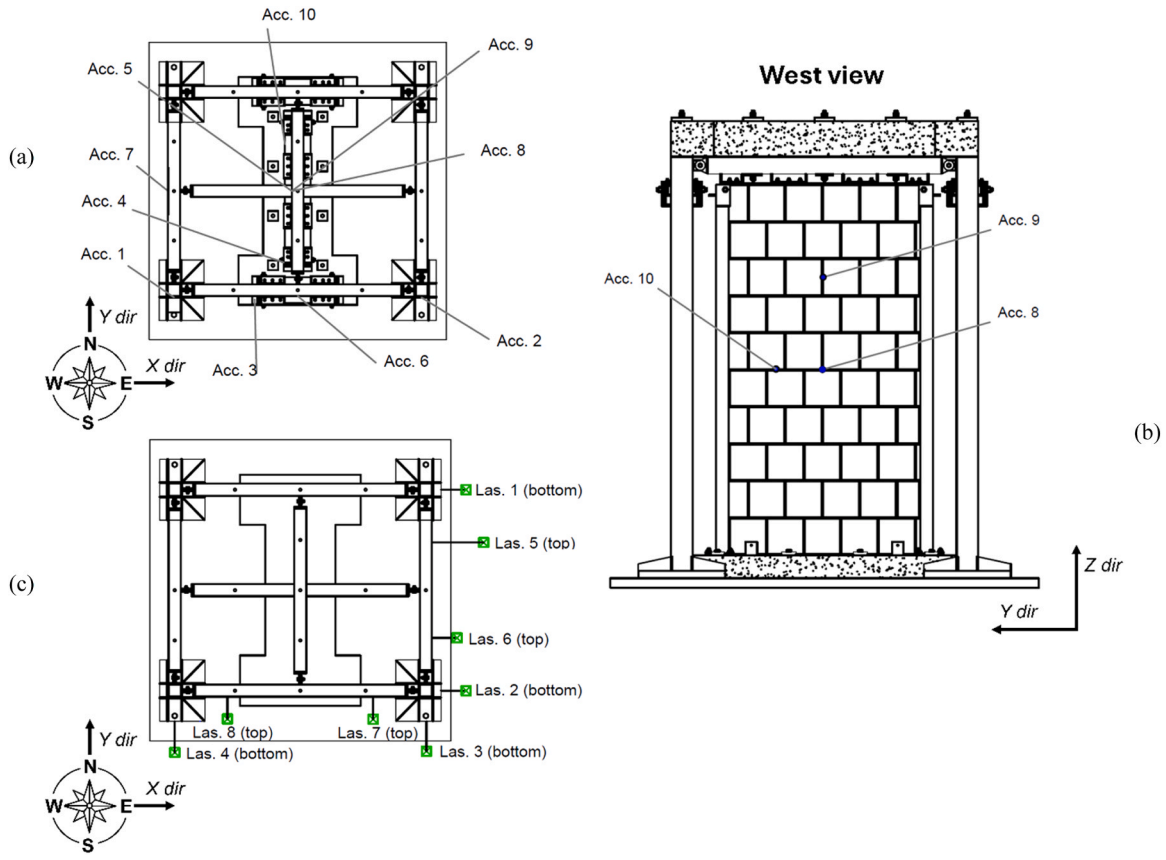

Fig. 5. Instrumentation arrangement: (a) accelerometer position in plain view, (b) accelerometer layout in lateral view, and (c) laser-optical sensor arrangement.

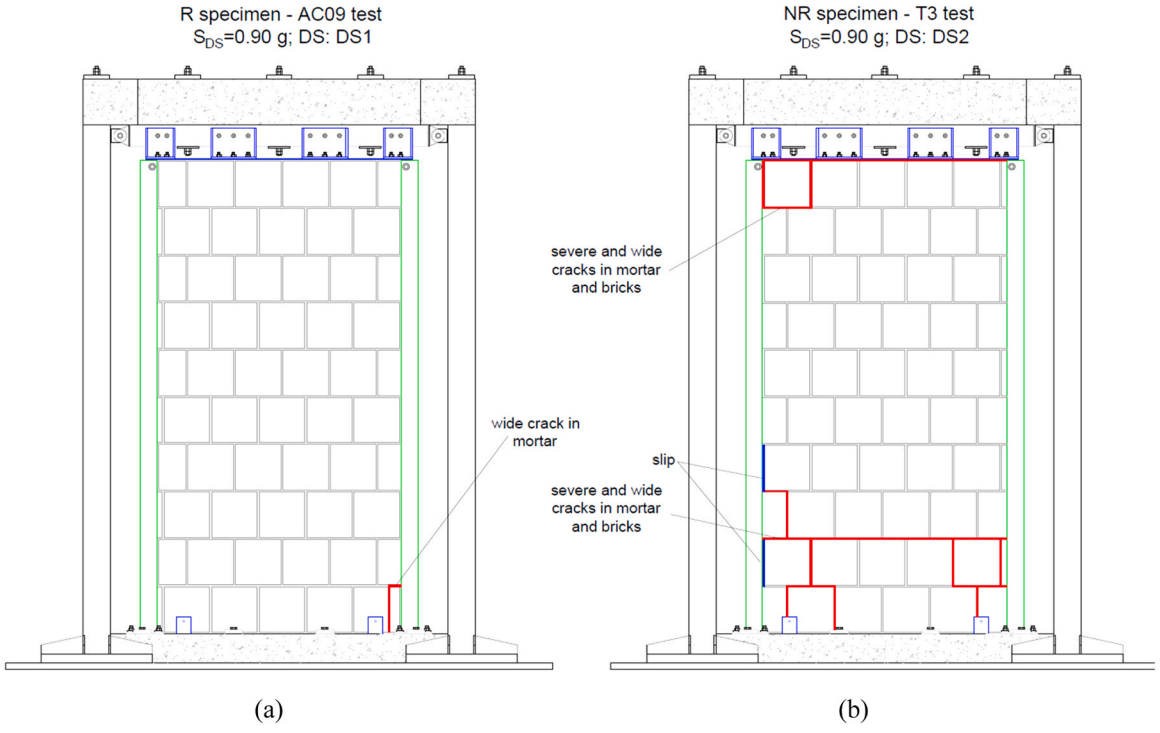

Fig. 6. Crack maps associated with (a) retrofitted (R) and (b) non-retrofitted (NR) partitions, corresponding to the same test intensity (S_{DS}=0.90 g). R and NR partitions achieved minor damage and moderate damage state (DS1 and DS2), respectively.

the partition panel was identified up to AC04 test, even though minor deformation of the foam layer was observed. This damage condition did not affect at all the integrity of the brick panels and did not represent a concern for the partition's performance. Corresponding to AC04 test (IDR along Y equal to 0.24 %), a horizontal hairline crack was observed in the bottom-left corner of the panel; this damage is associated with DS0 since the damage is negligible, as previously described. During AC05 test (IDR along Y equal to 0.35 %) and AC06 test (IDR along Y equal to 0.39 %), few and multiple hairline cracks, respectively, started to develop and extend, tending to involve all panel corners, even though the damage was still negligible (DS0) up to AC07 test (included) (IDR along Y direction equal to 0.49 %). Corresponding to AC08 test (IDR along Y direction equal to 0.56 %), cracks width increased, and hairline cracks developed into fine cracks, propagating out of the corner areas; this damage condition was associated with DS1 (minor damage). As the test intensity increased for AC09 (IDR along Y direction equal to 0.70 %), very few wide cracks tended to develop but they affected only one corner of the panel; therefore, the damage condition was still associated with DS1. Fig. 6a shows the damage pattern (crack map) associated with this latter condition (R partition), neglecting hairline and fine cracks.

The crack propagation process slightly evolved during the highest intensity test AC10 (Fig. 7) (IDR along Y direction equal to 0.84 %), but the wide partition panel did not reach moderate damage (DS2) despite S_{DS} was equal to 1.0 g, with peak table acceleration (PTA) along X and Y equal to 0.87 and 0.81 g, respectively. The final condition of the wide panel is depicted in Fig. 7a, where it can be observed that the only corner of the panel exhibited (minor) damage. In Table 4, PGA_{min} and PTA_{min} define the minimum PGA and PTA associated with the seismic input, respectively, over X and Y directions, which always correspond to Y direction values.

IDR_Y corresponds to the IDR associated with the in-plane response of the wide panel; PTA_{min} is associated with the actual recorded table responses, corresponding to the applied loading protocol, whereas PGA_{min} represents the (demand) PGA threshold correlated to PTA_{min} according to the protocol formulation (accounting for the building amplification [58]).

No visible damage was identified in the small partition panels up to AC04 test (IDR along X direction equal to 0.34 %). The first horizontal hairline crack was identified after AC04 test, and these cracks extended during AC05 and AC06 tests without visibly widening the crack opening.

Corresponding to AC07 test (IDR along X direction equal to 0.72 %), additional horizontal and vertical hairline cracks initiated in the lower part of a panel and, corresponding to AC08 test (IDR along X direction equal to 0.70 %), these cracks involved both panels; this damage is associated with DS0 (negligible damage). The width of these cracks

Fig. 7. Damage exhibited by the partition panels at the end of the incremental tests: (a) detail of the corner crushing for the wide partition panel (retrofitted (R) specimens), (b) detail of the wide sliding cracks in mortar in the joint between the bricks for the small partition panels (R specimens), and comparison between (c) R specimens and (d) non-retrofitted (NR) specimens [46].

Table 4
Damage assessment results associated with retrofitted (R) specimen and non-retrofitted (NR) specimen [46], considering the wide partition panel. PGA_{min} and PFA_{min} refer to minimum peak ground acceleration (PGA) and peak floor acceleration (PFA) measures along the horizontal directions in bidirectional tests. PFA corresponds to peak table acceleration (PTA) as the table represents the building floor. Peak frequency variation notes are related to the partition-frame system (Section 4.3.1).

S_{DS} [g]	R specimens test ID	NR specimens test ID	PGA_{min} [g]	PFA_{min} [g]	R specimens (wide panel) DS	R specimens (wide panel) Note	R specimens (wide panel) IDR_Y [%]	NR specimens (wide panel) DS	NR specimens (wide panel) Note	NR specimens (wide panel) IDR_Y [%]
-	***RAN1 X/Y***	***DYN1 X/Y***	-	-	-	**initial conditions**	-	-	**initial conditions**	-
0.10	AC01	-	0.02	0.07	DS0	no visible damage	0.09	-	-	-
0.20	AC02	-	0.05	0.16	DS0	no visible damage	0.12	-	-	-
0.30	AC03	T1	0.08	0.24	DS0	no visible damage	0.17	DS0	multiple hairline cracks (w<0.3 mm)	0.12
0.40	AC04	-	0.11	0.32	DS0	no visible damage	0.24	-	-	-
0.50	AC05	-	0.13	0.40	DS0	first horizontal hairline crack (w<0.3 mm)	0.35	-	-	-
-	-	***DYN2 X/Y***	-	-	-	-	-		**5% relative decrease (3% increase) in peak frequency along X (Y)**	-
0.60	AC06	T2	0.16	0.48	DS0	multiple hairline cracks (w<0.3 mm)	0.39	DS1	perimetrical wide crack (5 mm≤w<10 mm)	0.21
-	***RAN2 X/Y***	***DYN3 X/Y***	-	-		**22% (10%) relative decrease in peak frequency along X (Y)**			**14% (23%) relative decrease in peak frequency along X (Y)**	
0.70	AC07	-	0.20	0.59	DS0	multiple hairline cracks in all panel corners (w<0.3 mm)	0.49	-	-	-
-	***RAN3 X/Y***	-	-	-		**limited relative decrease in resonant frequencies**		-	-	-
0.80	AC08	-	0.22	0.67	DS1	fine cracks in all panel corners and propagating out (0.3 mm≤w<5 mm)	0.56	-	-	-
-	***RAN4 X/Y***	-	-	-		**limited relative decrease in resonant frequencies**		-	-	-
0.90	AC09	T3	0.25	0.75	DS1	fine cracks in all panel corners and propagating out (0.3 mm≤w<5 mm); few wide cracks at one corner (5 mm≤w<10 mm)	0.70	DS2	severe cracks at brick joints (10 mm≤w<20 mm); localized partition spalling	0.34
-	***RAN5 X/Y***	***DYN4 X/Y***	-	-		**4% (no) relative decrease in peak frequency along X (Y)**			**6% (10%) relative decrease in peak frequency along X (Y)**	-
1.00	AC10	-	0.28	0.84	DS1	fine cracks in all panel corners and propagating out (0.3 mm≤w<5 mm); few wide cracks at one corner (5 mm≤w<10 mm)	0.84	-	-	-
1.20	-	T4	0.34	1.01	-	-	-	DS3	extended severe cracks at brick joints (10 mm≤w<20 mm); severe/extended partition spalling; corner crushing	0.66
-	-	***DYN5 X/Y***	-	-	-	-	-		**2% (2%) relative decrease in peak frequency along X (Y)**	-
1.50	-	T5	0.42	1.27	-	-	-	DS3	extremely severe cracks (w≥20 mm); structural integrity significantly affected; unsafety condition	0.97

w: crack width.

tended to increase in tests AC09 (IDR along X direction equal to 0.92 %) and these became fine cracks, which propagated during this latter test and AC10 test (IDR along X direction equal to 1.24 %); these tests are associated with achievement of DS1. As for the wide partition, small partition panels did not reach moderate damage (DS2) following highest intensity test AC10 (Fig. 7b) and IDR equal to 1.24 %.

The exhibited damage is mostly related to the in-plane behavior of the partition, and no out-of-plane damage mechanisms were observed. Fig. 7c shows the final damage condition of the wide partition panel, and this demonstrates that the exhibited in-plane damage, which was minor up to very high seismic intensities, did not affect the structural integrity of the panels and it did not reduce the out-of-plane capacity of the panel. In particular, considering the wide panel that is more representative of real applications, the DS1 capacity of the tested partitions can conservatively be associated with the highest PGA_{min} and PTA_{min} associated with achievement of DS0, corresponding to 0.20 g and 0.59 g, respectively. The achievement of DS1 corresponds to PGA_{min} and PTA_{min} equal to 0.22 g and 0.67 g, respectively. DS2 achievement could be associated with PGA_{min} and PTA_{min} larger than 0.28 g and 0.84 g, respectively, which are the highest testes intensities, even though these capacities might potentially even be significantly higher than these latter thresholds.

The influence of the retrofitting on the partition damage and capacity was assessed by comparing R specimens observed damage and identified DSs with the results associated with NR specimens, focusing on the wide partition panel. Fig. 6 shows the comparison of R and NR partitions' response corresponding to a representative test intensity, i.e., S_{DS} equal to 0.90 g, focusing on wide and severe cracks. It can be observed that R partitions subjected to a PTA equal to 0.84 g (S_{DS} equal to 0.90 g) (Fig. 6a) sustained only low damage, limited to slight corner crushing (very few wide cracks), which corresponds to a minor damage state (DS1) and to OLS, as it is also discussed in Section 5. In contrast, NR partitions experienced minor damage (DS1) at lower intensities than R partitions (e.g., PTA equal to 0.48 g), as summarized in Table 2, and, more importantly, they exhibited a markedly more critical damage at S_{DS} equal to 0.80 g, characterized by horizontal cracks wider than 0.3 mm in the lower wall region, conditions consistent with a moderate damage state (DS2) and DLS (Fig. 6b), as also discussed in Section 5; moreover, NR partitions also exhibited slip cracks within the mortar joint between the edge bricks and the secondary frame columns. The damage condition achieved at the highest intensity tests is depicted Fig. 7 for both R and NR partitions.

Specifically, NR wide partition achieved DS1 and DS2 under a maximum IDR equal to 0.21 % and 0.34 %, respectively [46]. R wide partition did exhibit DS1 corresponding to a maximum IDR equal to 0.56 %, and, under an IDR equal to 0.84 % it did not exhibit DS2. Furthermore, NR wide partition exhibits DS3 under IDR equal to 0.66 %, whereas, as was discussed above, R partition did not even exhibit DS2 corresponding to 0.84 %. Table 4 shows the damage assessment results, focusing on PGA_{min} and PTA_{min} capacities associated with achieved DSs; dynamic identification tests refer to RAN (DYN) tests for R (NR) specimens, and seismic performance tests correspond to AC (T) tests,

respectively. DS identification related to NR specimens was based on the implementation of the DS criteria defined in this study, which are different from the one defined by Petrone et al. [46]. Tests 1–3 carried out in [46] correspond to AC03, AC06, and AC09, whereas tests 4 and 5 were associated with S_{DS} equal to 1.20 and 1.50 g, not performed in the current tests. Whereas NR exhibited multiple hairline cracks corresponding to PGA_{min} (PTA_{min}) equal to 0.08 g (0.24 g), R specimens still do not show visible damage up to PGA_{min} (PTA_{min}) equal to 0.11 g (0.32 g). DS1 is achieved corresponding to PGA_{min} (PTA_{min}) equal to 0.16 g (0.48 g) for NR specimens (wide crack), whereas DS1 PGA_{min} (PTA_{min}) capacity related to R specimens is equal to 0.22 g (0.67 g) (fine cracks in all panels corners and propagating out of them). The retrofitting produced an increment of 140 % and 39 % of maximum DS0 and minimum DS1 capacities, respectively, expressed in terms of PGA_{min} and PTA_{min}. As it was previously discussed, DS2 and DS3 were not exhibited by R specimens up to PGA_{min} (PTA_{min}) equal to 0.28 g (0.84 g), whereas DS2 is associated with PGA_{min} (PTA_{min}) equal to 0.25 g (0.75 g) for NR specimens. Therefore, the retrofitting intervention certainly improves the performance associated with DS2, whereas it might also affect DS3 capacities. However, performing further tests, at higher intensities, would have assessed the effectiveness of the retrofitting system also with regard to more severe damage conditions and limit states.

4.2. Partition-frame system accelerations and relative displacements

Peak accelerations recorded on the top of the main frame (peak frame top acceleration (PFTA)) and on shake table (PTA) and PFTA to PTA ratio are reported in Table 5, and peak relative displacement of the main frame (peak frame relative displacement (PFRD)) and IDR are reported in Table 6. PFTA and PFTA/PTA related to test AC10 are not reported since some registrations were defective in terms of signal acquisitions.

Fig. 8 depicts PFTA to PTA ratio and IDR related to retrofitted (R) specimens, tested in this study, and non-retrofitted (NR) ones, tested by Petrone et al. [46]. The differences identified in Fig. 8 are essentially due to the retrofitting intervention since the test frame and setup implemented in this study was the one used in [46]. It is worth recalling that the frame top response is associated with the whole tested system, which includes the three panels. R specimens presented PFTA/PTA higher than NR specimens, especially along X direction, showing that the retrofitting overall increases the acceleration amplification and that, as confirmed by the IDRs, in the test configuration, the retrofitted partitions are subjected to higher seismic demands: this is significant, as shown by Table 3, considering that the damage of the NR specimens was larger. PFTA/PTA ratio tends to decrease as PTA increases for all cases but R specimens along Y direction; in this latter case, the ratio does not have a regular pattern over the testing intensity and might be roughly considered to be constant over medium to high PTA values. Linear trends depicted in Fig. 8 were found to be fitting with good agreement PFTA/PTA vs. PTA responses associated with NR data, with coefficient of determination (r^2) equal to 0.76 and 0.87 along X and Y direction, respectively; for R data, the fitting quality is overall lower and more (less) satisfactory along X (Y) direction, with r^2 equal to 0.70 (0.57).

Table 5
Peak table acceleration (PTA), peak frame top acceleration (PFTA), and PFTA to PTA ratio along X and Y directions associated with incremental tests.

test ID	SDS [g]	PTA [g]		PFTA [g]		PFTA/PTA [-]	
		X dir	Y dir	X dir	Y dir	X dir	Y dir
AC01	0.10	0.09	0.07	0.24	0.22	2.81	2.98
AC02	0.20	0.18	0.16	0.56	0.46	3.09	2.87
AC03	0.30	0.29	0.24	0.78	0.67	2.73	2.75
AC04	0.40	0.37	0.32	0.92	0.84	2.48	2.63
AC05	0.50	0.47	0.40	1.17	1.00	2.47	2.53
AC06	0.60	0.57	0.48	1.36	1.27	2.40	2.64
AC07	0.70	0.64	0.59	1.47	1.54	2.31	2.63
AC08	0.80	0.74	0.67	1.61	1.73	2.18	2.58
AC09	0.90	0.82	0.75	1.89	1.97	2.31	2.63
AC10	1.00	0.91	0.84	NA	NA	NA	NA

Table 6
Peak frame relative displacement (PFRD) and interstory drift ratio (IDR) along X and Y directions associated with incremental tests.

test ID	SDS [g]	PFRD [mm]		IDR [%]	
		X dir	Y dir	X dir	Y dir
AC01	0.10	3.10	2.69	0.10	0.09
AC02	0.20	4.49	3.60	0.15	0.12
AC03	0.30	8.36	5.22	0.28	0.17
AC04	0.40	10.19	7.15	0.34	0.24
AC05	0.50	16.27	10.42	0.54	0.35
AC06	0.60	17.99	11.55	0.60	0.39
AC07	0.70	21.56	14.72	0.72	0.49
AC08	0.80	23.67	16.95	0.79	0.56
AC09	0.90	27.71	20.87	0.92	0.70
AC10	1.00	37.17	25.34	1.24	0.84

A highly regular response was exhibited by R and NR specimens in terms of IDR versus PTA along both directions. In particular, a second-order polynomial trend was found to fit at best all curves, with r^2 larger than 0.97. However, linear trends depicted in Fig. 8 supply fitting r^2 just lower than the polynomial order ones (r^2 larger than 0.95) in all cases. Therefore, linear trend can be considered as a reference. R specimens-frame system was found to be more deformable than NR. The increase in IDR to PTA linear best-fit gradient due to the retrofit resulted in 40 % and 22 % along X and Y direction, respectively; the higher influence along X direction is consistent with the higher ratio between the linear extension of the retrofit intervention and the surface of the partition panels. The increase in acceleration amplification due to the retrofitting (Fig. 8a) was associated with an increase in IDR to PTA gradient of the system (Fig. 8b); this stresses the complexity of simultaneous in-plane and out-of-plane response of the partition panels and the combination of the three partitions responses in the setup. The reason behind the higher (dynamic) deformability of the retrofitted system, in terms of IDR vs. PTA response, is associated with the large deformability of the foam layer, while its larger IDR to PTA gradient could be related to the larger damage suffered by the NR system, becoming more significant as the acceleration grows, conditioning the response trend in terms of damping, as will be shown in the next section. The retrofit did not significantly alter the relative deformability of the partitions in different directions.

4.3. Dynamic identification and damage interpretation

4.3.1. Partition-frame system

The transfer function method [59] was used to assess the dynamic properties of the system, considering the results of RAN tests. The transfer function (TF) associated with the response of the partition-frame system are depicted in Fig. 9; the curves were assessed considering shake table and frame top acceleration responses as input and output signals, respectively. RAN1X (RAN1Y) peak natural frequencies, related to the undamaged conditions, are larger than the ones associated with other RAN2X (RAN2Y) to RAN5X (RAN5Y) tests, which are lightly different.

RAN1X test was conducted before the AC01 test ($S_{DS} = 0.10$ g), while the RAN2X test followed the AC06 test (SDS = 0.60 g). In the X direction, the frequency decreased by about 22 %, from 6.2 Hz (RAN1X) to 4.9 Hz (RAN2X). Similarly, RAN1Y test took place before the AC01 test, and the RAN2Y test followed the AC06 test. In the Y direction, the frequency dropped by about 10 %, from 5.9 Hz (RAN1Y) to 5.3 Hz (RAN2Y).

These frequency decreases are mostly associated with the damage initiation process affecting both wide and narrow panels corresponding to AC03 test. Note that Table 2 correlates the dynamic identification

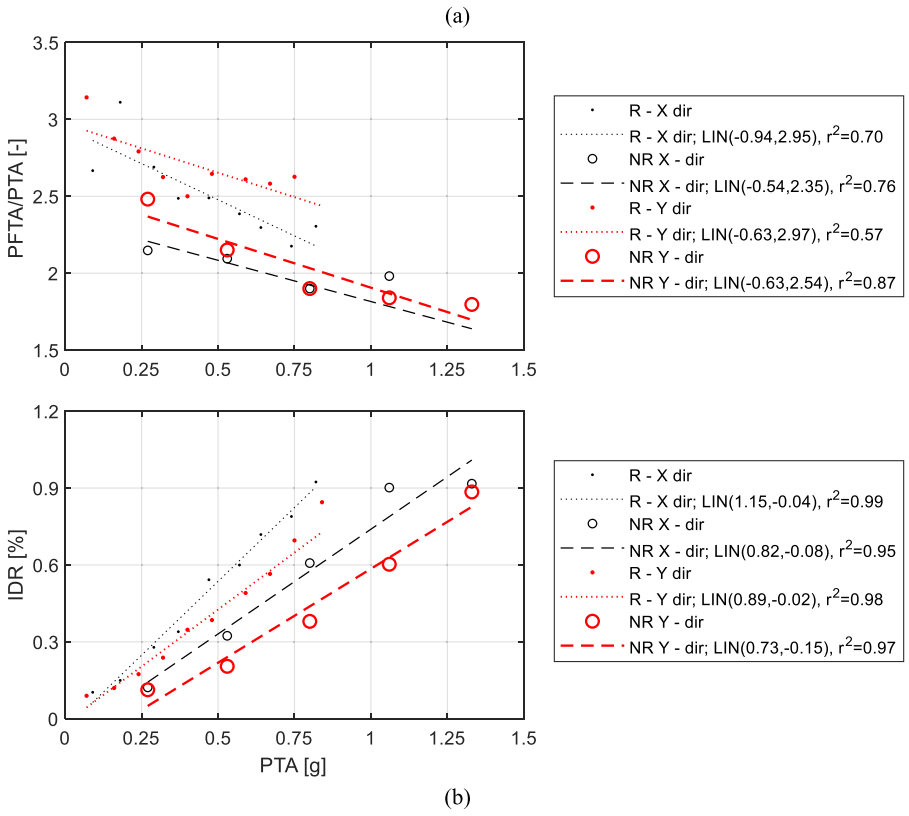

Fig. 8. (a) Peak frame top acceleration to peak table acceleration ratio (PFTA/PTA) and (b) interstory drift ratio (IDR) associated with incremental peak table acceleration (PTA), related to retrofitted (R) and non-retrofitted (NR) specimens.

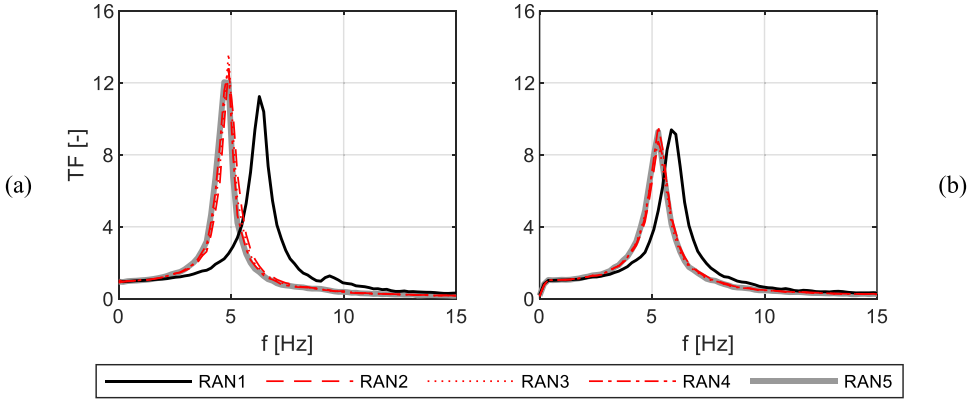

Fig. 9. Transfer function (TF) associated with response of the partition-frame system along (a) X and (b) Y directions for all random (RAN) tests; shake table and frame top acceleration responses are considered as input and output signals, respectively.

results (partition-frame system frequency variations) to the observed damage, as it is discussed below. The onset of the abovementioned cracking process early reduces the (in-plane) stiffness of both wide and narrow panels, and this is consistent with the observed decrease in natural frequency (Fig. 9). However, the arrangement variation of the setup (e.g., main frame and frame that hosts the partition panels) most probably also contributed to the abovementioned decrease in frequency. According to the lightly different frequency peaks of the following tests (Fig. 9), once the damage process initiated, the contribute of the stiffness of both panels on the partition-frame system is not significant, even though limited decreases in resonant frequency are overall observed. As is discussed in Section 4.3.2, a more significant influence of damage to peak frequencies is identified considering the local out-of-plane response of the panel. RAN5X test frequency was about 4 % lower than RAN4X one, meaning that AC09 test affected the frequency response of the system along X direction, even though not in a significant manner. The damaged condition frequency, slightly lower than 5 Hz, is significantly larger than the bare frame (BF) one, equal to about 4 Hz, and this proves that the specimens and the related interfaces still increase the overall stiffness of the setup, being affected by minor damage; this did not happen regarding NR specimens [46] since the presented damaged natural frequencies are slightly larger than BF ones, demonstrating that the partition system did not retain any significant lateral stiffness due to the accumulate damage.

Table 7 reports a comparison among the natural frequencies (f) related to BF and both NR and R specimens partition-frame systems (undamaged conditions) and the percentage frequency variation (Δf) among the different cases. The presence of both NR and R partitions

Table 7
Undamaged frequency analysis results: natural frequency (f) related to bare frame (BF) and partition-frame systems (retrofitted (R) and non-retrofitted (NR) specimens) and percentage frequency variation (Δf) associated with NR to BF, R to BF, and R-NR cases.

direction	f [Hz]			Δf [%]		
	f_{BF}	f_{NR}	f_R	$\frac{f_{NR}-f_{BF}}{f_{NR}}$	$\frac{f_R-f_{BF}}{f_R}$	$\frac{f_R-f_{NR}}{f_R}$
X	3.83	8.01	6.25	+ 52	+ 39	-28
Y	4.04	7.62	5.86	+ 47	+ 31	-30

significantly increases the natural frequency of the system (Δf = +52 %/+47 % for NR and +39 %/+31 % for R specimens along X/Y direction), whereas the retrofitting sensibly decreases the frequency if compared with the non-retrofitted partitions (Δf = −28 %/-30 % along X/Y direction). This latter outcome is also consistent with IDR to PTA gradient assessed in Section 4.2 (Fig. 8b), which tends to increase due to the retrofitting, compatible with higher deformability of the retrofitted system. The decrease in natural frequency and increase in deformability are associated with higher acceleration amplification due to the retrofitting, as previously discussed (Fig. 8a).

Table 2 shows that the major frequency drop observed passing from RAN1 to RAN2 tests is associated with multiple hairline cracks forming (in the wide panel) but not with DS1 achievement; RAN2 tests were performed after the attainment of IDR_y equal to about 0.4 %. This confirms that the presence of the polyurethane foam at the interface between the panel and the secondary frame allows relatively larger in-plane interstory deformations and affects the stiffness of the panel-to-interface system preventing the cracking damage of the panel itself. The earliest achievement of DS1 is associated with limited resonant frequency decreases, visible considering TF shape than frequency peak, whereas a more significant, even though not major, drop is observed passing within subsequent DS1 conditions. This suggests that the in-plane panel-to-interface stiffness decrease is governed by the deformation at the interface and not by the panel cracking evolution. Additionally, multiple hairline cracks within the panel, even though negligible in terms of damage, might affect the dynamic properties of the panel-to-interface system (i.e., frequency) in a more significant manner than slightly wider cracks evolving from these latter hairline ones. This latter observation, related to the multiple hairline cracks within the panel, is also compatible with NR results, which show that multiple hairline crack formation is associated with (minor) decrease in frequency.

The damping of the partition-frame systems was assessed according to the energetic method (EM) [46,59], considering the partition-frame system as a single-degree-of-freedom (SDOF) system. An equivalent viscous damping ratio (ξ) was computed from the hysteretic energy per cycle, overall incremental tests, and the median values associated with each incremental test are shown in Fig. 10 along (a) X and (b) Y directions. For R specimens, ξ tends to increase over the low to medium intensity incremental tests and approximately remains constant over the medium to high intensity. In particular, at the lowest intensity test (PTA lower than 0.1 g), ξ is equal to about 4 % and 1.5 % along X and Y directions, respectively, and it raises up to about 9 % at higher intensities (i.e., PTA equal to about 0.4 g), remaining approximately constant over higher intensities. The regular increase in damping observed over the low to medium intensity tests is mainly due to the damage exhibited by the specimens, but it is also reasonably associated with the minor modification of the setup arrangement.

Fig. 10 shows that, for R specimens, ξ significantly increases under lower intensity tests up to AC04 tests (the fourth dot in Fig. 10), and, after this latter test, ξ tends to be constant or slightly increases as the test intensity grows. This latter damping response is consistent with the evolution of the fundamental frequency (Fig. 9), which shows a major frequency decrease corresponding to AC04 test (between RAN1 and RAN2) and negligible variations under higher intensities (from RAN3 upwards). This suggests that incipient damage conditions have a major effect on the dynamic properties of the partitions, even though it does not affect their capacity and performance. ξ is affected by the partition damage process more gradually than the natural frequency. For R specimens, whereas the undamaged damping associated with X direction is slightly larger than the one related to Y direction, for medium to high intensity tests, the damping does not seem to depend on the loading direction.

Fig. 10 also depicts the NR results, which exhibit a trend along X direction that is different from the one related to R specimens. For NR specimens, damping ratio slightly decreases over low to medium intensities along X direction, reaching a value quite similar to the R one associated with high intensities (about 8.5 %). Along the Y direction, the NR damping ratio evolves similarly to the R one, but it is lower during low-to-medium intensity tests (PTA < 0.6 g) and higher during medium-to-high intensity tests (PTA > 0.6 g). The final damping ratio related to NR specimens is slightly lower than 11 %. An interpretation of the damping evolution associated with NR specimens was provided in [46], and this is omitted for the sake of brevity. In the light of the above-mentioned results along the more representative Y direction, the retrofitting increases the damping capacity of the specimen for low to medium seismic intensities; as expected, as the seismic intensity grows and the NR specimen is heavily damaged while the R specimen is lightly damaged, the damping capacity of the former one overpasses the damping capacity of the latter one.

Overall, damping ratios associated with R partitions are comparable with the ones related to NR ones, proving that the solution enhances the seismic capacity without significantly altering the damping capacity.

4.3.2. *Partition panel*

The out-of-plane dynamic properties of the wide partition panel were assessed considering the response at the center of the panel as an output

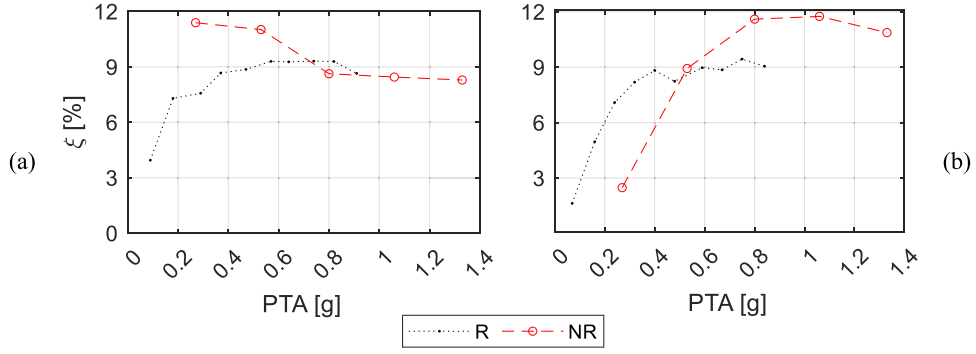

Fig. 10. Damping ratio (ξ) evaluation according to the energetic method (EM) corresponding to incremental tests related to retrofitted (R) and non-retrofitted (NR) specimens along (a) X and (b) Y direction.

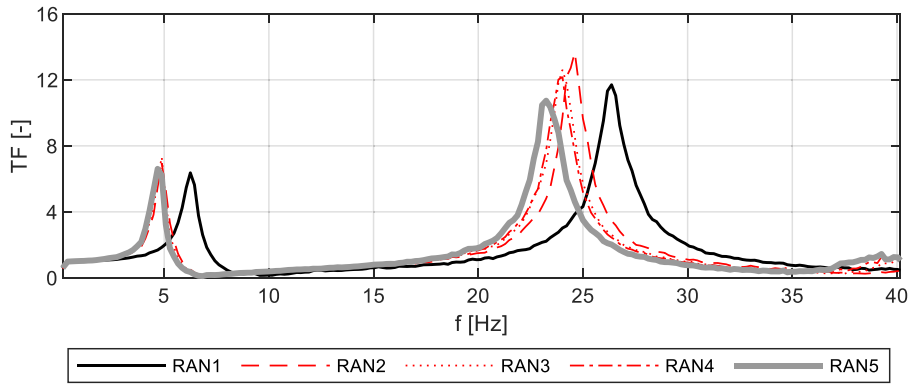

Fig. 11. Transfer function (TF) associated with (RANX tests) out-of-plane response (along X direction) of wide partition panel; shake table and wide partition panel midpoint acceleration responses are considered as input and output signals, respectively.

(Acc. 8), along X direction, considering the dynamic identification (RAN) tests. TF curves associated with the wide partition panel are depicted in Fig. 11.

Two peak sets can be identified in Fig. 11: (1) the lower frequency peaks (about 5.0 Hz) are associated with the (global) response of the test set-up (partition-frame system) since it corresponds to the frequency peak depicted in Fig. 9a; (2) the higher frequency peaks are related to the (local) out-of-plane vibrational response of the wide partition along X direction (natural frequency f), which also presents ordinates that are significantly higher than the lower frequency peaks. Table 8 reports the evolution of the peak frequency associated with the local out-of-plane vibration mode of the wide panel for all tests. As expected, f decreases along the incremental testing procedure, due to the damage accumulated by the partition panel.

The overall resonant frequency decrease is mostly associated with RAN1X to RAN2X interval, as it was observed accounting for the partition-frame system, and, minorly but still sensibly passing from RAN2X to RAN3X and from RAN4X to RAN5X. With regard to RAN3X to RAN4X resonant frequency variation, it should be specified that (a) this is not clearly visible only accounting for the peak frequency and that (b) more accurate dynamic identification methods, such as best curve-fitting method that accounts for the TF shape rather than the only peak, e.g., [60,61], would highlight a more significant variation. However, detailed dynamic identification analyses fall beyond the scope of this paper, especially considering that the evidenced transfer curve and frequency peak evolution is compliant with the observed damage.

The abovementioned decreases in resonant (and peak) frequency are reasonably due to the previously discussed in-plane damage and perimetrical detachment of the foam. Differently from the frequency evolution associated with the partition-frame system (Fig. 9a), the out-of-plane frequency decreases according to a more gradual pattern, still compliant with the one related to the partition frame system along X direction. This is meaningful since the partition-frame system response along X direction is not only affected by the out-of-plane behavior of the wide panel but also by the in-plane response of the small ones; whereas the frequency evolution depicted in Fig. 11 only accounts for the out-of-plane response of the wide panel, which is significantly more indicative of the (in-plane and perimetrical) accumulated damage of the wide panel.

ξ was assessed through half-power bandwidth method applied with regard to TF [59] since the out-of-plane displacement of the wide partition was not monitored. This method was developed for SDOF systems, but it was often applied in the literature to assess multiple degree of freedom (MDOF) systems [62]. In this specific case, the out-of-plane response of the (wide) partition panel can reasonably be associated with a SDOF response. The method was calibrated considering the partition-frame system damping assessment (Section 4.3.1), which was performed through the energetic method. For the partition-frame system, the damping ratios evaluated considering the half-power bandwidth method were found to be consistent with the one assessed through EM, with discrepancy not exceeding 10 %; they are not reported for sake of brevity. Table 8 shows that ξ associated with the wide partition panel along out-of-plane (X) direction overall slightly increases along the test progression, and the final value is about 25 % larger than the initial one. Whereas this increasing trend is consistent with the results associated with the partition-frame system, the out-of-plane damping ratios are significantly lower, confirming that the damping is mostly associated with the in-plane behavior of the partition rather than with the out-of-plane one.

Table 8
Natural frequency (f) and damping ratio (ξ) evolution associated with wide partition panel along out-of-plane (X) direction.

ID test	RAN1X	RAN2X	RAN3X	RAN4X	RAN5X
f [Hz]	26.4	24.6	24.0	24.0	23.2
ξ [%]	2.13	2.00	2.20	2.36	2.68

f and ξ associated with undamaged NR partitions are equal to 31.2 Hz and 1.92 %, respectively [46]. It can be observed that the retrofitting intervention determined a decrease in frequency (about 15.4 %) and increase in damping ratio (about 12.1 %) associated with wide partition panel along out-of-plane (X) direction.

For elastic damped SDOF, frequency f is proportional to the product of pulsation ω (i.e., $\sqrt{k/m}$, where k and m are elastic stiffness and mass, respectively) and $\sqrt{1-\xi^2}$; accordingly, a lower frequency can be associated with lower stiffness and/or higher damping ratio, for fixed mass. R partition system reasonably presents an elastic stiffness that is about 46 % lower than NR one, considering the out-of-plane frequency and damping response previously depicted. This different stiffness, i.e., R stiffness about 46 % lower than NR one, is related to the different panel to secondary frame interface constraint: NR panel was fixed to the secondary frame columns' hollow, whereas R panel was connected to them through foam. This response is also compatible with the response of the partition-frame system (Section 4.2) associated with IDR to PTA linear best-fit gradient variation (Section 4.3.1). In particular, IDR to PTA linear gradient (deformability measure) associated with R was found to be larger than the NR one, along both directions, recalling that the partition-frame system accounts for the simultaneous response of all three panels (wide panel out-of-plane and small panels in-plane responses).

4.4. Component amplification factor

The component amplification factor defines the acceleration amplification factor due to the dynamic response of NEs under dynamic

actions, and this is often referred to as a_p or CAF in literature studies [63–66] and codes [67,68]. This factor can be experimentally assessed by dividing peak acceleration on the element (namely, peak component acceleration (PCA)) to the reference input peak acceleration, which for a SDOF element can be simply defined as the peak acceleration applied at its fix constraint. Considering a SDOF element fixed at the building floor, the abovementioned reference input peak acceleration can be referred to PFA, whereas for elements that have multiple connections and/or cannot be simply defined by SDOF systems, there is not a univocal identification of input peak acceleration.

CAF is essential for the estimation of the seismic demands on acceleration-sensitive NEs [50]. The out-of-plane response of the investigated partition is associated with the seismic inputs at two consequent building floors, represented by shake table and frame top. In particular, the partition panels are subjected to both shake table and top frame accelerations and displacements. Therefore, CAF is assessed by considering two different approaches, referring to CAF_1 and CAF_2. CAF_1 is defined as PCA divided by PA*, which is assumed as the linear interpolation acceleration between PTA and PFTA along the story height. CAF_2 corresponds to PCA to PTA ratio. PCA, CAF_1, and CAF_2 were assessed considering the wide panel at both middle height point (Acc. 8) and (width midpoint) ¾ height point (Acc. 9), as it is shown in Fig. 12.

PCA approximately increases linearly as PTA grows up to PTA equal to 0.47 g (AC05 test), and it decreases passing to PTA equal to 0.57 g (AC06 test); after this test, PCA again increases with PTA even though with a slightly higher PCA to PTA gradient. As PTA increases, the discrepancy between 3/4 height point and middle height point PCA grows; discrepancy is approximately negligible for the lowest intensity test and becomes equal to about 0.4 g at the highest intensity test.

CAF_1 does not significantly vary as PTA grows for both 3/4 height point and middle height point of the wide panel, ranging between 0.9 and 1.3 without exhibiting a clear trend; in particular, CAF_1 mean value is approximately equal to 1.1 for both panel's points. As it was expected, CAF_2 exhibits a completely different trend as PTA grows: (a) it gradually decreases, from values equal to 2.5–3, up to PTA equal to 0.37 g (AC04), reaching values equal to about 2–2.5; (b) passing from PTA equal to 0.37 g to PTA equal to 0.47 g (AC05), it increases to values equal to about 2.3–2.6; (c) for highest test intensities, CAF_2 does not significantly vary as PTA grows, with values within 1.6–2.3, but for a given panel's point the values are essentially constant. Plotting CAF_1 as a function of PA* does not change the trend identified considering PTA, as it was expected, and further comments are omitted for the sake of brevity. Depending on the approach of estimation of CAF, both value range and influence of the test intensity change. However, the values and tendencies provided can be useful for an expeditious but robust assessment of the seismic demands on the investigated partition, for comparison and practical purposes.

4.5. 4.5 Hysteretic behavior

Fig. 13 depicts the hysteretic curves of the partition-frame system for AC03, AC06, and AC09 tests, corresponding to PTA equal to 0.29 g (0.24 g), 0.57 g (0.48 g), and 0.82 g (0.75 g) along X (Y) direction, respectively. It is recalled that this hysteretic response is mostly representative of the in-plane behavior of (a) both small panels along X and (b) wide panel along Y direction.

As the test intensity grows, the overall hysteretic fuse inclination lightly tends to decrease as the loading and unloading stiffness lightly decreases, and this is more significant along X direction, or rather, for the in-plane response of the two small panels. This evidence shows that, overall, the specimen lightly tends to become more deformable as the test intensity grows. Along both directions and especially along Y direction, a hardening response is noted over larger displacements; the displacement level corresponding to the onset of the hardening tends to increase as the test intensity increases and the (minor) damage accumulates. The hardening trend for increasing deformation is probably due to increasing compressive strain given by the vertical column in contact with the partition, showing the activation of an inclined strut, as suggested by Preti et al. [69]. Furthermore, the hysteretic fuse related to Y direction (in-plane response of wide panel) is lightly wider than the one associated with X direction (in-plane response of small panels).

Fig. 14 shows a comparison of hysteretic curves related to R and NR specimens for same intensity tests, i.e., AC03-T1, AC06-T2, and AC09-

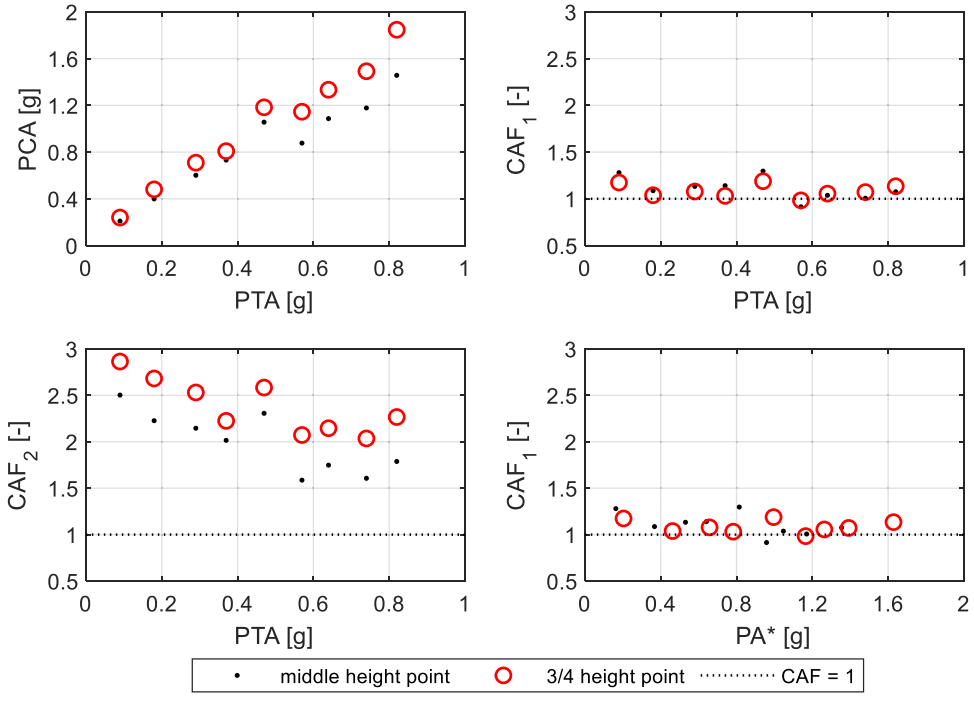

Fig. 12. Peak component acceleration (PCA) and component amplification factors CAF_1 and CAF_2, as a function of peak table acceleration (PTA), and CAF_1 as a function of interpolated peak acceleration (PA*).

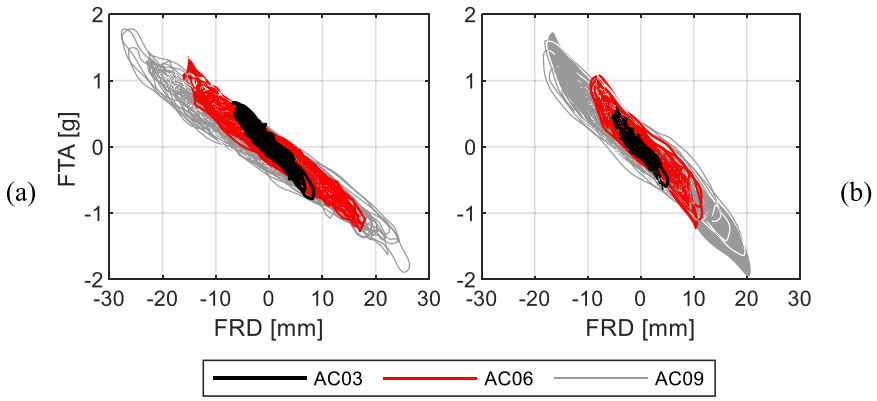

Fig. 13. Hysteretic curves: frame top acceleration (FTA) as a function of frame relative displacement (FRD) for AC03, AC06, and AC09 tests, along (a) X and (b) Y directions (retrofitted (R) specimens). Peak table acceleration (PTA) is equal to 0.29 g (0.24 g), 0.57 g (0.48 g), and 0.82 g (0.75 g) along X (Y) direction.

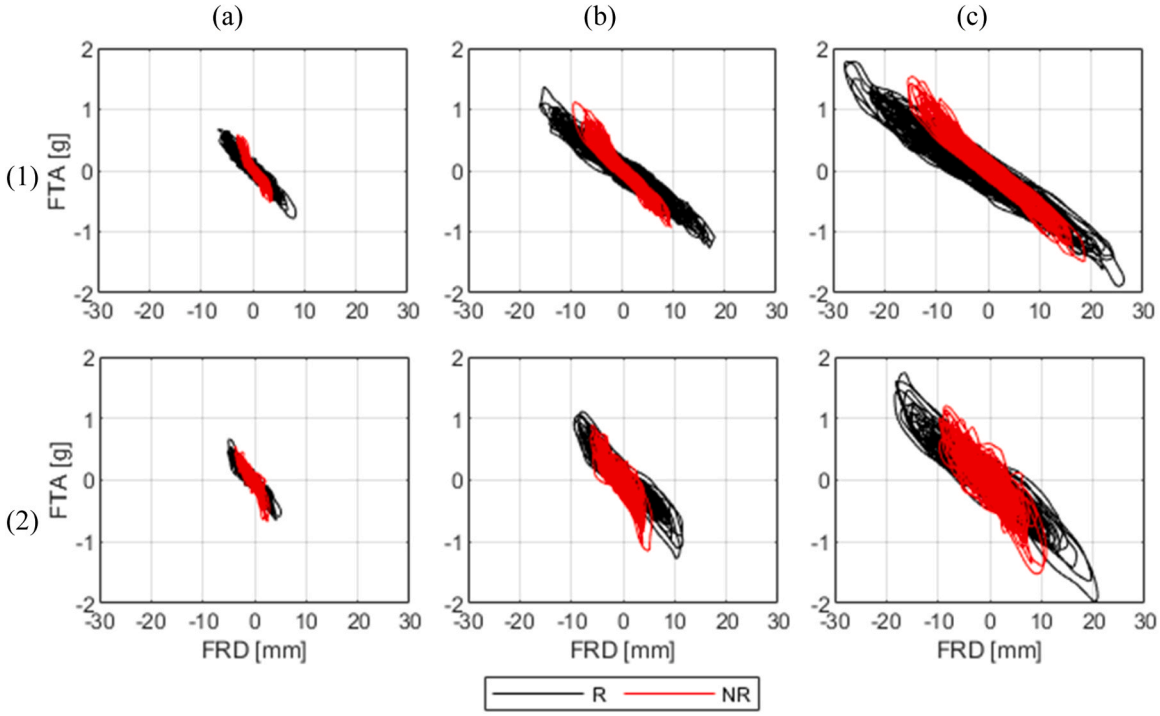

Fig. 14. Hysteretic curves: frame top acceleration (FTA) as a function of frame relative displacement (FRD) considering retrofitted (R) and non-retrofitted (NR) [46] partitions for (a) AC03-T1, (b) AC06-T2, and (c) AC09-T3 tests, along (1) X and (2) Y directions. Peak table acceleration (PTA) is equal to 0.29 g (0.24 g), 0.57 g (0.48 g), and 0.82 g (0.75 g) along X (Y) direction.

T3. Since low intensity tests, the hysteretic curves related to R and NR specimens exhibit significant differences, and this can be clearly observed with regard to both loading/unloading stiffness and hysteretic fuse. NR specimens present more significant hardening response in the loading branches and higher unloading stiffness; these differences are due to the retrofitting intervention since the presence of the foam layer between the partition panels and the vertical frame elements significantly reduces the corresponding panel to frame strut mechanism influence on the response. The abovementioned effects on the hysteretic response explain the lower damage observed in the case of retrofitted specimens, as it was observed in Section 4.1.

The hysteretic response of the R and NR specimens could represent as a reference for calibrating simplified analytical models of partition walls, allowing the incorporation of the foam layer's influence. In particular, models based on the compressive strut mechanism, traditionally developed for masonry infills, could be adapted to partitions and could be provided with zero-length springs at the strut-to-frame interfaces (e.g., [70,71]). These phenomenological models could be calibrated using insights derived from the experimental hysteresis curves, and the experimental data developed in this study are made available upon request to the corresponding author.

5. Seismic safety assessment

5.1. Outline

The assessment implements the performance-based earthquake engineering (PBEE) approach [72–74]. In particular, seismic safety assessment, referred to a quantitative comparison of demand and capacity measures associated with the investigated NEs, could be implemented considering three orders/levels of parameters, applied (1) on the NE, e.g., PCA, (2) at the building floor/support of installation of NE, e.g., PFA, and (3) at the foundation of the structure, e.g., PGA. A more detailed discussion can be found in literature studies and codes [73–75].

In the specific case, PGA could be used as an IM for seismic assessment since each test, or, equivalently, each test response of the specimens under dynamic excitations, is referred to a PGA level, according to the shake table protocol (AC156 [48]); IM (i.e., PGA) is consistently correlated to EDP (i.e., PFA), to DM (i.e., PCA), to the observed specimen damage, and to the conventional DS.

5.2. Experimental capacity

Seismic capacity corresponding to DS_i can be expressed in terms of measures that are associated with the experimental achievement of DS_i. According to the incremental testing procedure and to the damage assessment (i.e., Table 4), DS_i can be considered to be achieved for PGA-PFA-IDR measures that range from (a) the largest PGA-PFA-IDR values causing DS_{i-1} achievement and (b) the smallest PGA-PFA-IDR values corresponding to DS_i attainment. The upper bound capacity thresholds is typically considered in the literature [16,76] and is referred to in this study, and the lower conservativity is reasonably balanced by (a) reliability of the testing procedure and (b) relatively narrow intensity increments. Table 9 reports the seismic capacities of R and NR partitions assessed accordingly.

DS2 capacity associated with R partitions was not achieved during the tests, and the value reported in Table 9 represents a lower bound, which is likely to be significantly lower than the actual DS2 capacity condition, according to the experimental evidence regarding the observed damage (Section 4.1).

5.3. Case studies and demand assessment

Case studies include (a) high, medium, and low seismicity sites in Italy, corresponding to L'Aquila, Naples, and Milan sites and (b) importance class (IC) [77] (or risk category (RC) [78]) II and IV buildings [47]. Seismic demand was estimated for case study buildings/sites according to the Italian building code NTC 2018 [47,79], assuming rigid soil conditions (Table 10).

Seismic demands on IC II (IV) buildings was associated with a reference period (V_R) equal to 50 (200 years), according to the Italian building code [47]; V_R is defined as the product of nominal life (V_N), equal to 50 and 100 years for Class II and IV buildings, and building class factor, equal to 1 and 2, respectively. T_R associated with the considered LSs was assessed considering the exceedance probability within V_R (P_{V_R}) provided by [47], corresponding to 81 %, 63 %, and 10 % for OLS, DLS, and LSLS, respectively, according to Eq. (5). T_R resulted in 30, 50, and 475 years for IC II buildings, and in 120, 201, and 1989 years for IC IV buildings.

$$T_R = \frac{V_R}{\ln(1 - P_{V_R})} \tag{5}$$

5.4. Safety assessment results

Fig. 15 shows the results of the seismic safety assessment, for (a) L'Aquila, (b) Naples, and (c) Milan sites, referring to (1) R and (2) NR specimens, considering PGA as an assessment measure. OLS, DLS, and LSLS conditions were verified corresponding to DS1, DS2, and DS3 achievement, respectively.

Considering OLS, R partitions provide DS0 (OLS*) and DS1 capacity PGA values (0.20 and 0.28 g, respectively) that are larger than most severe condition demand measure (V_R equal to 200 years, T_R equal to 120 years, and demand PGA equal to 0.15 g), corresponding to high seismicity (L'Aquila) and IC IV buildings (Fig. 15a.1), whereas NR partition fails by a great amount the OLS condition considering DS0 (OLS*) and slightly comply considering DS1 capacity. For less severe conditions (Naples, Milan IC IV buildings and all sites IC II buildings), R partitions satisfy by a great amount the safety conditions, whereas NR partitions generally satisfy the safety conditions but might be unsafe in case of Naples and IC IV buildings, considering DS0.

Regarding DLS, R partitions satisfy the most severe condition since DS2 capacity PGA (larger than 0.28 g) is certainly significantly larger than the related demand measure (T_R equal to 201 years, and demand PGA equal to 0.19 g at L'Aquila), whereas NR partitions are likely to provide unsafe DS2 capacities.

Finally, NR partitions fail to satisfy LSLS condition associated with the most severe demand measure (T_R equal to 1989 years, and demand PGA equal to 0.41 g), since DS3 capacity (0.34 g) is significantly lower than the related demand level; DS2 and DS3 capacities associated with R partitions were not identified but these are likely to be higher than the one related to NR partitions. It should be noted that, considering IC II buildings and L'Aquila site, R partitions still exhibit DS1 under LSLS demands.

Regarding deformation capacities, differently from NR partitions, R ones provide IDR capacities (Table 2 and Fig. 8) significantly larger than drift requirements typically referred to infills and partitions (e.g., 0.5 % [47,77]) and are likely to provide capacities compatible with ductile partitions and infills (e.g., 0.75 % [47,77]). Therefore, the seismic performance of R partitions is satisfactory also regarding the deformation behavior, and this potentially result in major economic advances regarding the dimensioning of RC members, which is typically based on deformation targets associated with NEs [47,77].

Table 9
Seismic capacity criteria associated with retrofitted (R) and non-retrofitted (NR) partitions. NA: not available.

DS	R			NR		
DS1	PGA $\geq$ 0.22 g	PFA $\geq$ 0.67 g	IDR $\geq$ 0.56 %	PGA $\geq$ 0.16 g	PFA $\geq$ 0.48 g	IDR $\geq$ 0.21 %
DS2	PGA $>$ 0.28 g	PFA $>$ 0.84 g	IDR $>$ 0.84 %	PGA $\geq$ 0.25 g	PFA $\geq$ 0.75 g	IDR $\geq$ 0.34 %
DS3	NA	NA	NA	PGA $\geq$ 0.34 g	PFA $\geq$ 1.01 g	IDR $\geq$ 0.66 %

6. Cost and effectiveness analysis

6.1. Simplified cost analysis

Economic aspects play a significant role in the definition and implementation of retrofitting interventions regarding infills and partitions [40,80]. Therefore, a simplified cost analysis was performed considering a case study building derived from a literature study [16]. The reference building is a regular RC frame serving as a residential unit, with three stories and two apartments for each story. The area dimension of each apartment is equal to about 103 m^2.

The costs were computed according to current practice, average price lists, and they were corroborated by a small size construction company, also referring to the realization of the testing setup. Costs account for construction workers' costs and raw material costs, and both costs also include costs related to supplementary, transportation, and landfill disposal activities; 10 % profit is added considering the final cost. Costs are meant to be VAT included. The detailed methodology implemented for the cost analysis is reported in the Appendix

A simplified estimation of the required work time for retrofitting all partitions in the apartment, considering a team of three level I workers working 8 h per day, results in approximately 2.33 working days, also including a 20 % increase to account for preparation, cast-off activities, and other potential time commitments (as it was done for related costs), resulting in about 0.022 working days/m^2 per apartment area.

The results of the simplified cost analysis are reported in Table 11. About 50 % of intervention costs are associated with worker costs. The total cost for an apartment results in about 2512 €, which averaged on apartment area is equal to about 24.2 €/m^2. This cost is clearly lower than alternative partition retrofitting interventions, as well as it is quite reduced if compared with typical unitary costs of apartment restyling

Table 10
Seismic demand acceleration at bedrock (a_g) associated with operativity limit state (OLS), damage limitation limit state (DLS), and life safety limit state (LSLS) for importance class (IC) II and IV buildings, according to the Italian building code [47].

Site	Longitude	Latitude	a_g [g]					
			IC II			IC IV		
			OLS	DLS	LSLS	OLS	DLS	LSLS
L'Aquila	13.399	42.349	0.079	0.104	0.261	0.153	0.191	0.415
Naples	14.268	40.854	0.045	0.059	0.168	0.094	0.120	0.259
Milan	9.186	45.465	0.019	0.024	0.051	0.034	0.039	0.072

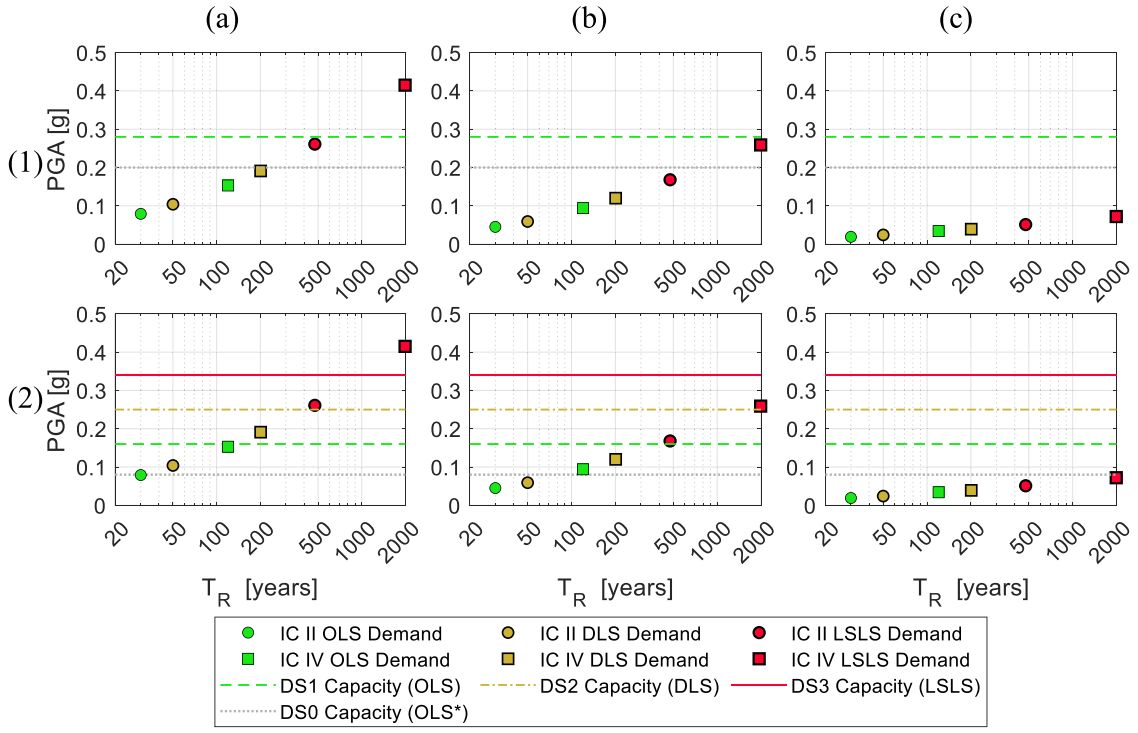

Fig. 15. Seismic demand and capacity associated with peak ground acceleration (PGA). Demand is assessed considering (a) L'Aquila, (b) Naples, and (c) Milan sites, accounting for return period (T_R) associated with operativity limit state (OLS), damage limitation limit state (DLS), and life safety limit state (LSLS) for importance class (IC) II and IV buildings, according to the Italian building code NTC 2018 [47,79]. Capacity refers to (1) retrofitted (R) and (2) non-retrofitted (NR) specimens.

Table 11
Results of simplified cost analysis referred to the case study building and architectural layout [16]. All costs include 10 % profit.

Averaged material cost per retrofitting length*	Averaged work cost per retrofitting length*	Total cost per partition development length**	Total cost per partition development area***	Total cost per apartment area	Total cost for apartment
[€/m]	[€/m]	[€/m]	[€/m^2]	[€/m^2]	[€]
19.18	15.48	100.5	31.70	24.20	2512

* Total panel to column/slab interface length; ** total longitudinal partition length; *** total lateral partition area.

refurbishment in Italy (e.g., 250–600 €/m^2).

6.2. Repair cost analysis

A repair cost analysis was carried out to provide quantitative insights into the seismic effectiveness of the developed retrofitting solutions. The methodology implemented in [16] was extended to the retrofitted partitions, referring to the same building and architectural layout considered for the cost analysis. In particular, repair costs (R_c) associated with four T_R earthquakes were estimated for the retrofitted partitions and compared to non-retrofitted ones, in the framework of multiple-stripe analysis (MSA) carried out in [81]. Retrofitted and compared to non-retrofitted partitions are referred to as R-HB and NR-HR partitions, respectively. For comparison purposes, R_c related to standard plasterboard (SP) and innovative plasterboard (IP) partitions, derived from [16], are also reported. Fig. 16 illustrates R_c associated with the case study apartment related to abovementioned partition types, corresponding to (a) AQ and (b) NA. For 50 years T_R, corresponding to DLS demand for IC II buildings, NR-HR allows to save almost 500 €, but for 100 years T_R repair costs due to NR-HZ exceed 3000 €, whereas R-HB ones are still null. Initial costs associated with implementation of the developed retrofitting intervention during building construction become almost negligible since the slot can be realized by partition construction rather than from partition cutting.

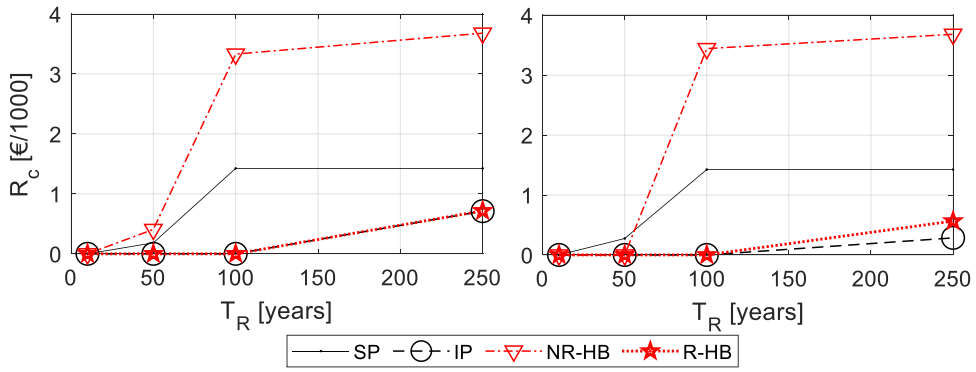

Fig. 16. Repair costs (R_c) for the case study apartment associated with four return period (T_R) earthquakes for standard plasterboard (SP), innovative plasterboard (IP), non-retrofitted hollow brick (NR-HR), and retrofitted hollow brick (R-HB) partitions; SP, IP, and NR-HR R_c are derived from [16].

7. Discussion remarks and conclusion

7.1. Outline

The study develops and experimentally tests a novel rapid and effective retrofitting solution for infill and partition panels, based on an interconnection of panels and surroundings by means of a layer of self-expanding polyurethane foam. This detailing variant overcomes the limitations of traditional gap-based solutions, typically only suitable for initial construction, providing enhanced seismic performance.

7.2. Methodological robustness and generalizability

The experimental tests comply with AC156 protocol [48], which ensures standardized methods, comparability with other studies using the same procedure, and reliable capacity thresholds. However, the purpose of the paper is not merely a seismic qualification, but rather the implementation of a robust experimental program to evaluate the seismic performance of the proposed technical solution using state-of-the-art scientific approaches. In particular, PBEE framework is applied to assess both the seismic response and capacity of the tested partitions [72–74].

The study quantitatively investigates the dynamic properties and key response parameters of the partitions, including transfer curves linked to global and local modes, fundamental frequencies and damping ratios, component amplification factors (through alternative approaches), hysteretic behavior, and observed damage classified into conventional damage states essential for PBEE. Capacity thresholds are related to both damage states and PBEE limit states, seismic demands are estimated according to regulations [47,79], seismic safety checks are carried out, and a cost and loss/repair analysis is performed.

In conclusion, while AC156 provides a standardized and reliable testing platform, the work extends far beyond qualification by extracting governing parameters, identifying performance and damage thresholds, and integrating these into a PBEE-based assessment. The resulting methodologies, experimental results, and cost-repair analysis yield technical insights and practical guidance for implementation of retrofitting intervention, seismic capacity estimations, and approximate implementation/repair costs, respectively.

7.3. Damage and seismic performance

The experimental evidence proves that the retrofitting intervention is effective in terms of observed damage and hysteretic response. Section 4.1 shows that the retrofitted partition panels present absent or negligible damage (DS0) corresponding to PTA equal to about 0.6 g, and this damage condition does not affect the operativity performance; conversely, corresponding to the same seismic intensity, the non-retrofitted partitions present minor damage (DS1), which potentially affects the operativity performance. The retrofitted partitions only present minor damage (DS1) corresponding to significantly high seismic intensities, e.g., PTA larger than 0.8 g, whereas the non-retrofitted partitions exhibit severe damage (DS2), which becomes extremely severe (DS3) corresponding to PTA equal to about 1.0 g.

The developed retrofitting technique significantly increases both DS1 and DS2 capacities (and potentially also DS3 ones). Retrofitted partitions can accommodate major in-plane deformation without exhibiting damage conditions that affect the operativity and damage limitation performance. The retrofitting intervention and the (minor) exhibited in-plane damage did not weaken the out-of-plane resistance; on the contrary, the out-of-plane mechanism was found to be less critical for the retrofitted partitions than for non-retrofitted ones since the in-plane deformation do not produce in-plane damage that could cause out-of-plane response mechanisms. Corresponding to the earliest damage condition achievement, the observed frequency reductions, mainly due to increased deformability of the polyurethane foam rather than visible damage, suggest that subtle degradation mechanisms may develop in the connections without apparent warning signs. However, experimental evidence indicates that such phenomena do not compromise the seismic performance up to moderate-to-high intensity levels. This confirms the robustness and reliability of the proposed retrofitting solution, even under cumulative dynamic demands.

The acceleration amplification factor was assessed considering two alternative approaches, and the linear interpolation alternative was found to be relatively effective to capture the out-of-plane acceleration amplification along the intensity increase. The hysteretic response was characterized, and it evidenced further the different nature of the cyclic response of the retrofitted panels, as compared to the non-retrofitted ones. The presence of the foam layer between the panels and the test frame nullifies or significantly mitigates the detrimental frame to partition interaction, with regard to the compression strut mechanisms that typically activate in traditional brick infills and partitions.

The tests investigated the response of the retrofitted partitions up to high seismic intensities, e.g., demand PGA equal to about 0.3 g. Performing higher intensity tests would have revealed whether the retrofitting would have improved the performance regarding damage limitation and life safety limit states. Further studies will test the effectiveness of the retrofitting also with regard to these more severe conditions.

7.4. Seismic safety assessment

The improved capacity of the retrofitted partitions potentially satisfies severe demand conditions, as was demonstrated in Section 5, differently from traditional (non-retrofitted) solutions. The systematic implementation of the developed retrofitting technique potentially produces major impacts on overall building capacities and performances associated with the operativity and the damage limitation conditions

and limit states. NEs play an important role on the definition of the overall building design and assessment, with regard to both deformability (in-plane response) and inertial effects (out-of-plane response), for IC II facilities, considering both DLS and LSLS, and for IC IV buildings also considering OLS. Furthermore, preventing severe damage of the abovementioned elements also mitigates the significance of potential human losses, as the severe damage of those elements also threatens human life.

7.5. Practical feasibility and economic aspects

The technical solution can be rapidly implemented by non-specialized construction workers, and, considering the case study building/apartment (about 103 m^2 area), a team of three workers would need about 8 working days for the whole apartment. The technique is economically convenient, and most costs are associated with work rather than with materials. Time and cost commitments are significantly cheaper than other traditional techniques, even though further studies will focus on economic effectiveness in more quantitative manners. The implementation of the developed retrofitting detailing, especially in the context of building construction, might determine major economic savings.

7.6. Limitations of the study and future developments

Even though the retrofitting solution was confirmed to be seismically effective, it should be noted that it was provided and tested as a technical detailing and not as a theoretical-based or analytical design option. The results are influenced by the specific test setup, particularly the boundary conditions of the partition panels. A limited number of specimens was tested, and this limits the extrapolation of the findings with regard to different specimen features. Loading history uncertainty, associated with building-to-building and record-to-record variability, was not accounted for since the compliance with the AC156 protocols fosters a high level of reliability and representativeness. Moreover, since moderate to severe damage conditions were not observed up to spectral response acceleration at short periods (S_{DS}) equal to 1 g, associated capacities were not identified.

Further studies will focus on the development of advanced numerical models by implementing the experimental data developed in the paper. The experimental data will be provided upon request to the corresponding authors, in order to maximize the potential output of the study, fostering development of advanced models of retrofitted hollow brick partitions.

The proposed technical detailing could be also applied as a design/construction technique for new buildings, following further investigations. For new buildings, the foam would be applied during the partition construction, without the need to implement a cut at the panel to frame interface, easing further the intervention process.

CRediT authorship contribution statement

Danilo D'ANGELA: Writing – review & editing, Writing – original draft, Visualization, Software, Methodology, Investigation, Formal analysis, Data curation, Conceptualization. **Andrea PROTA:** Writing – review & editing, Validation, Project administration, Funding acquisition, Conceptualization. **Gennaro MAGLIULO:** Writing – review & editing, Validation, Supervision, Resources, Project administration, Methodology, Investigation, Funding acquisition.

Declaration of Competing Interest

The authors declare that they have no known competing financial interests or personal relationships that could have appeared to influence the work reported in this paper.

Acknowledgement

The paper was funded by (1) the Italian Ministry of University and Research (MUR) in the framework of the Italian project PRIN 2020 YKY7W4 "ENRICH: ENhancing the Resilience of Italian healthCare and Hospital facilities", (2) MAPEI S.p.A. in the framework of the agreement MAPEI-DIST, and (3) the Italian Department of Civil Protection (DPC) in the framework of the national project DPC – ReLUIS 2024–2026 WP17: "Elementi non strutturali". Prof. Alberto Balsamo is thanked for supporting the experimental tests and Dr. Francesca Celano is thanked for supporting the experimental tests and the data elaborations.

Appendix

A.1 Instrumentation details

Table A1 reports the instrumentation details, referring to Section 2.4.

Table A1
Description of the sensor instrumentation: accelerometers (Acc.) and laser sensors (Las.)

sensors	monitored element	sensor location (measuring direction(s))
Acc. 1	south-west main frame column	column's base (X,Y,Z)
Acc. 2	south-east main frame column	column's base (X,Y,Z)
Acc. 3	south-west secondary frame column	column's base (X,Y,Z)
Acc. 4	south secondary frame beam to column connection	beam's midpoint (X,Y,Z)
Acc. 5	secondary frame beam	beam's midpoint (X,Y,Z)
Acc. 6	south main frame beam	beam's midpoint (X,Y,Z)
Acc. 7	west main frame beam	beam's midpoint (X,Y,Z)
Acc. 8	wide partition panel	panel's midpoint (X,Y,Z)
Acc. 9	wide partition panel	width: midpoint; height: ¾ panel's height (X,Y,Z)
Acc. 10	wide partition panel	width: ¾ panel's width; height: midpoint (X,Y,Z)
Las. 1	north-east main frame column	column's base (X)
Las. 2	south-east main frame column	column's base (X)
Las. 3	south-east main frame column	column's base (Y)
Las. 4	south-west main frame column	column's base (Y)
Las. 5	east main frame beam	¾ beam's width point, closer to north (X)
Las. 6	east main frame beam	¾ beam's width point, closer to south (X)
Las. 7	south main frame beam	¾ beam's width point, closer to east (Y)
Las. 8	south main frame beam	¾ beam's width point, closer to west (Y)

A.2 Technical definition of damage states

This section provides the technical definition of damage states (DSs) defined in Section 3. Damage conditions that only affect the aesthetics of the panel (cosmetic damage such as negligible finish damage or hardline cracks with width lower than 0.3 mm), were associated with absent or negligible damage (DS0). Damage conditions that potentially affect the functioning of the facility, or of the adjacency of the panel, not necessitating major repair interventions, were associated with DS1, corresponding to OLS condition. Technical DS1 condition includes fine cracks (width within 0.3 and 5 mm) affecting relatively extended areas of the panel (e.g., more than 50 %) or wider cracks (with widths within 5 and 10 mm) in reduced areas (e.g., less than 10 %) or superficial localized partition spalling in reduced areas (e.g., less than 10 %).

More severe damage conditions that refer to more significant economic losses and repair interventions that do not potentially affect global integrity of the partition panel and safety of occupants were correlated to DS2, corresponding to the achievement of DLS conditions. DS damage conditions include wider cracks (width within 5 and 10 mm) affecting extended areas of the panels or more severe cracks (width within 10 and 20 mm) in reduced areas (e.g., less than 10 %) or localized partition spalling in reduced areas (e.g., less than 10 %). More severe damage conditions that potentially affect global integrity of the partition panel or safety of occupants, representing a potential threat to life, in addition to critical economic losses/repair interventions, refer to DS3, associated with achievement of requirements related to LSLS condition. DS3 damage conditions include severe cracks (width within 10 and 20 mm) in extended areas (e.g., more than 50 %) or severe/extended partition spalling or extremely severe cracks (width $>$ 20 mm) or any other potentially critical damage condition.

A.3 Simplified cost analysis

This section describes the methodology implemented for the simplified cost analysis discussed in Section 6.1. Worker costs were computed by valorizing estimated construction workers time at a 22.69 €/h rate. This rage was derived from the 2023 Italian Directorate Decree of the Ministry of Labor and Social Policies [82], and it refers to level I worker, i.e., non-specialized, in Rome area. As a matter of fact, the retrofitting intervention, as previously discussed, consists in basic construction activities, and it can be implemented by low expertise workers. The work time commitments were set equal to double times needed for the realization of the tested specimens in the laboratory to take into account the implementation of a real construction site.

Case study partitions are meant to be retrofitted at (a) vertical interfaces between panels and columns/structural elements and (b) horizontal interfaces between panels and slabs. For all work construction activities but supplementary/transportation/disposal ones, the interventions associated with upper half part of the vertical retrofitting (panel to column interface) and interventions related to (upper) horizontal retrofitting (panel to slab interface) were assumed to be equal two times the ones related to the bottom half part of the vertical retrofitting. The retrofitting interventions include the following construction steps: longitudinal slot realization, application of polyurethane foam, and finishing, and this latter step accounts for foam application cleaning, cutting, leveling, plastering, and painting/cosmetic finishing.

Hour work costs associated with these three steps are set equal to 1.89, 0.75, and 3.78 €/m for the bottom retrofitting (meter unit is referred to slot intervention length), and a 20 % cost increment was applied to take into account preparation, cast-off activities, and other potential time commitments. The material costs associated with application of polyurethane foam and finishing are set equal to 1.07 and 3.00 €/m for both bottom and upper applications, respectively (meter unit is referred to intervention length). The construction work and material costs associated with supplementary, transportation and landfill disposal activities are assumed to be equal to 3.78 and 10 €/m, respectively, and these costs were also incremented by 20 %.

Data availability

Data will be made available on request.

References

[1] Achour N, Miyajima M, Kitaura M, Price A. Earthquake-induced structural and nonstructural damage in hospitals. Earthq Spectra 2011;27:617–34. https://doi.org/10.1193/1.3604815.

[2] Masi A, Santarsiero G, Gallipoli MR, Mucciarelli M, Manfredi V, Dusi A, et al. Performance of the health facilities during the 2012 Emilia (Italy) earthquake and analysis of the Mirandola hospital case study. Bull Earthq Eng 2014;12:2419–43. https://doi.org/10.1007/s10518-013-9518-4.

[3] Ceferino L, Mitrani-Reiser J, Kiremidjian A, Deierlein G, Bambarén C. Effective plans for hospital system response to earthquake emergencies. Nat Commun 2020; 11:4325. https://doi.org/10.1038/s41467-020-18072-w.

[4] Lee T, Kato M, Matsumiya T, Suita K, Nakashima M. Seismic performance evaluation of non-structural components: drywall partitions. Earthq Eng Struct Dyn 2007;36:367–82. https://doi.org/10.1002/eqe.638.

[5] Sucuoğlu H. Implications of masonry infill and partition damage in performance perception in residential buildings after a moderate earthquake. Earthq Spectra 2013;29:661–7. https://doi.org/10.1193/1.4000147.

[6] Tapia-Hernández E, Geneş MC, Guerrero-Bobadilla H. Structural behavior of hospitals during the Kahramanmaraş earthquake of February 6, 2023. Earthq Spectra 2025;41:1589–615. https://doi.org/10.1177/87552930241298678.

[7] Taghavi S., Miranda E. Response assessment of nonstructural building elements. University of California, Berkeley: Pacific Earthquake Engineering Research Center; 2003.

[8] De Risi MT, Del Gaudio C, Verderame GM. A component-level methodology to evaluate the seismic repair costs of infills and services for Italian RC buildings. Bull Earthq Eng 2020;18:6533–70. https://doi.org/10.1007/s10518-020-00944-7.

[9] Fierro E.A., Miranda E., Perry C.L.. Behavior of Nonstructural Components in Recent Earthquakes. AEI 2011, Oakland, California, United States: American Society of Civil Engineers; 2011, p. 369–77. https://doi.org/10.1061/41168(399)44.

[10] Devin A, Fanning PJ, Pavic A. Modelling effect of non-structural partitions on floor modal properties. Eng Struct 2015;91:58–69. https://doi.org/10.1016/j.engstruct.2015.02.021.

[11] Ning N, John Ma Z, Zhang P, Yu D, Wang J. Influence of masonry infills on seismic response of RC frames under low frequency cyclic load. Eng Struct 2019;183: 70–82. https://doi.org/10.1016/j.engstruct.2018.12.083.

[12] Vicente RS, Rodrigues H, Varum H, Costa A, Mendes da Silva JAR. Performance of masonry enclosure walls: lessons learned from recent earthquakes. Earthq Eng Eng Vib 2012;11:23–34. https://doi.org/10.1007/s11803-012-0095-3.

[13] Yön B, Onat O, Öncü ME. Earthquake damage to nonstructural elements of reinforced concrete buildings during 2011 van seismic sequence. J Perform Constr Facil 2019;33:04019075. https://doi.org/10.1061/(ASCE)CF.1943-5509.0001341.

[14] Perrone D, Calvi PM, Nascimbene R, Fischer EC, Magliulo G. Seismic performance of non-structural elements during the 2016 Central Italy earthquake. Bull Earthq Eng 2019;17:5655–77. https://doi.org/10.1007/s10518-018-0361-5.

[15] Del Vecchio C, Di Ludovico M, Pampanin S, Prota A. Repair costs of existing RC buildings damaged by the L'Aquila earthquake and comparison with FEMA P-58 predictions. Earthq Spectra 2018;34:237–63. https://doi.org/10.1193/122916EQS257M.

[16] Magliulo G, D'Angela D, Lopez P, Manfredi G. Nonstructural seismic loss analysis of traditional and innovative partition systems housed in code-conforming RC frame buildings. J Earthq Eng 2021:1–28. https://doi.org/10.1080/13632469.2021.1983488.

[17] Petrone C, Magliulo G, Lopez P, Manfredi G. Out-of-plane seismic performance of plasterboard partition walls via quasi-static tests. Bull N Z Soc Earthq Eng 2016;49: 125–37. https://doi.org/10.5459/bnzsee.49.1.125-137.

[18] Amer S, Hamoush S, Abu-Lebdeh T. In-plane performance of gypsum board partition wall systems subjected to cyclic loadings. J Constr Steel Res 2016;124: 23–36. https://doi.org/10.1016/j.jcsr.2016.05.013.

[19] Fiorino L, Bucciero B, Landolfo R. Evaluation of seismic dynamic behaviour of drywall partitions, façades and ceilings through shake table testing. Eng Struct 2019;180:103–23. https://doi.org/10.1016/j.engstruct.2018.11.028.

[20] Furtado A, Rodrigues H, Arêde A, Varum H. Simplified macro-model for infill masonry walls considering the out-of-plane behaviour: macro-model for Infill Walls Considering the Out-of-plane Behaviour. Earthq Eng Struct Dyn 2016;45:507–24. https://doi.org/10.1002/eqe.2663.

[21] Mohammad Noh N, Liberatore L, Mollaioli F, Tesfamariam S. Modelling of masonry infilled RC frames subjected to cyclic loads: state of the art review and

modelling with OpenSees. Eng Struct 2017;150:599–621. https://doi.org/10.1016/j.engstruct.2017.07.002.
[22] Sorace S, Bidoli N, Terenzi G. Glazed-level dissipative brace incorporation in a gym building. Structures 2024;68:107184. https://doi.org/10.1016/j.istruc.2024.107184.
[23] Mucedero G, Perrone D, Monteiro R. Nonlinear static characterisation of masonry-infilled RC building portfolios accounting for variability of infill properties. Bull Earthq Eng 2021;19:2597–641. https://doi.org/10.1007/s10518-021-01068-2.
[24] Sorace S, Costoli I, Terenzi G. Seismic assessment and dissipative bracing retrofit-based protection of infills and partitions in RC structures. Eng Struct 2023;281:115781. https://doi.org/10.1016/j.engstruct.2023.115781.
[25] Bianchi S, Ciurlanti J, Perrone D, Filiatrault A, Costa AC, Candeias PX, et al. Shake-table tests of innovative drift sensitive nonstructural elements in a low-damage structural system. Earthq Eng Struct Dyn 2021;50:2398–420. https://doi.org/10.1002/eqe.3452.
[26] Preti M, Bettini N, Migliorati L, Bolis V, Stavridis A, Plizzari GA. Analysis of the in-plane response of earthen masonry infill panels partitioned by sliding joints: In-plane Response of Earthen Masonry Infill Panels with Sliding Joints. Earthq Eng Struct Dyn 2016;45:1209–32. https://doi.org/10.1002/eqe.2703.
[27] Magliulo G, Zito M, D'Angela D. Dynamic identification and seismic capacity of an innovative cleanroom with walkable ceiling system. Bull Earthq Eng 2024;22:3287–321. https://doi.org/10.1007/s10518-024-01895-z.
[28] Etemadi A, Balkaya C. The role of masonry infills on the interstory drift demand of reinforced concrete frames. Soil Dyn Earthq Eng 2024;180:108599. https://doi.org/10.1016/j.soildyn.2024.108599.
[29] Eren N, Brunesi E, Nascimbene R. Influence of masonry infills on the progressive collapse resistance of reinforced concrete framed buildings. Eng Struct 2019;178:375–94. https://doi.org/10.1016/j.engstruct.2018.10.056.
[30] Dolšek M, Fajfar P. The effect of masonry infills on the seismic response of a four astorey reinforced concrete frame—a probabilistic assessment. Eng Struct 2008;30:3186–92. https://doi.org/10.1016/j.engstruct.2008.04.031.
[31] Morandi P, Hak S, Milanesi RR, Magenes G. In-plane/out-of-plane interaction of strong masonry infills: From cyclic tests to out-of-plane verifications. Earthq Eng Struct Dyn 2022;51:648–72. https://doi.org/10.1002/eqe.3584.
[32] Mazza F, Donnici A. In-plane-out-of-plane single and mutual interaction of masonry infills in the nonlinear seismic analysis of RC framed structures. Eng Struct 2022;257:114076. https://doi.org/10.1016/j.engstruct.2022.114076.
[33] Jin W, Zhai C, Zhang M, Liu W, Wei Y, Xie L. Experimental investigation on the in-plane and out-of-plane interaction of isolated infills in RC frames. Eng Struct 2023;293:116569. https://doi.org/10.1016/j.engstruct.2023.116569.
[34] Furtado A, Teresa De Risi M. Recent findings and open issues concerning the seismic behaviour of masonry infill walls in RC buildings. Adv Civ Eng 2020;2020:9261716. https://doi.org/10.1155/2020/9261716.
[35] Di Trapani F, Di Benedetto M, Petracca M, Camata G. Local infill-frame interaction under seismic loads: investigation through refined micro-modeling. Eng Struct 2024;315:118088. https://doi.org/10.1016/j.engstruct.2024.118088.
[36] Verderame GM, Ricci P, De Risi MT, Del Gaudio C. Experimental assessment and numerical modelling of conforming and non-conforming RC frames with and without infills. J Earthq Eng 2019:1–42. https://doi.org/10.1080/13632469.2019.1692098.
[37] Braga F, Manfredi V, Masi A, Salvatori A, Vona M. Performance of non-structural elements in RC buildings during the L'Aquila, 2009 earthquake. Bull Earthq Eng 2011;9:307–24. https://doi.org/10.1007/s10518-010-9205-7.
[38] Bhatta J, Dhakal RP, Sullivan TJ, Bartlett J, Pring G. Seismic performance of internal partition walls with slotted and bracketed head-tracks. J Earthq Eng 2023;27:3435–70. https://doi.org/10.1080/13632469.2022.2137709.
[39] Furtado A, Rodrigues H, Arêde A, Varum H. Experimental tests on strengthening strategies for masonry infill walls: a literature review. Constr Build Mater 2020;263:120520. https://doi.org/10.1016/j.conbuildmat.2020.120520.
[40] Sousa L, Monteiro R. Seismic retrofit options for non-structural building partition walls: Impact on loss estimation and cost-benefit analysis. Eng Struct 2018;161:8–27. https://doi.org/10.1016/j.engstruct.2018.01.028.
[41] Huang B, Chen S, Lu W, Mosalam KM. Seismic demand and experimental evaluation of the nonstructural building curtain wall: a review. Soil Dyn Earthq Eng 2017;100:16–33. https://doi.org/10.1016/j.soildyn.2017.05.025.
[42] Milanesi RR, Morandi P, Manzini CF, Albanesi L, Magenes G. Out-of-plane response of an innovative masonry infill with sliding joints from shaking table tests. J Earthq Eng 2022;26:1789–823. https://doi.org/10.1080/13632469.2020.1739173.
[43] Huang W, Niu X, Zhang C, Ling B, Wu S, Deng X, et al. Experimental and analytical studies of infill wall with sliding joints considering a door opening. Earthq Eng Struct Dyn 2024;53:2162–84. https://doi.org/10.1002/eqe.4108.
[44] Gatto MPA, Lentini V, Castelli F, Montrasio L, Grassi D. The use of polyurethane injection as a geotechnical seismic isolation method in large-scale applications: a numerical study. Geosciences 2021;11:201. https://doi.org/10.3390/geosciences11050201.
[45] Gatto MPA, Montrasio L, Berardengo M, Vanali M. Experimental analysis of the effects of a polyurethane foam on geotechnical seismic isolation. J Earthq Eng 2022;26:2948–69. https://doi.org/10.1080/13632469.2020.1779871.
[46] Petrone C, Magliulo G, Manfredi G. Shake table tests for the seismic assessment of hollow brick internal partitions. Eng Struct 2014;72:203–14. https://doi.org/10.1016/j.engstruct.2014.04.044.
[47] Ministero delle Infrastrutture e dei Trasporti. D.M. del 17/01/2018 – "Aggiornamento delle Norme tecniche per le Costruzioni 2018" NTC 2018 (in Italian) 2018.
[48] International Code Council Evaluation Service (ICC-ES). AC156 Acceptance Criteria for the Seismic Qualification of Nonstructural Components. Brea, California, USA: 2020.
[49] Magliulo G, Petrone C, Capozzi V, Maddaloni G, Lopez P, Manfredi G. Seismic performance evaluation of plasterboard partitions via shake table tests. Bull Earthq Eng 2014;12:1657–77. https://doi.org/10.1007/s10518-013-9567-8.
[50] Zito M, Nascimbene R, Dubini P, D'Angela D, Magliulo G. Experimental seismic assessment of nonstructural elements: testing protocols and novel perspectives. Buildings 2022;12:1871. https://doi.org/10.3390/buildings12111871.
[51] Ente Nazionale Italiano di Unificazione. UNI EN 771-1:2015. Specifica per elementi per muratura - Parte 1: Elementi di laterizio per muratura. 2015.
[52] International Code Council. 2018 IBC code and commentary. 2018.
[53] American Society of Civil Engineers, editor. ASCE 7-16. Minimum design loads for buildings and other structures. Reston, Va: American Society of Civil Engineers: Structural Engineering Institute; 2017.
[54] De Santis S, AlShawa O, de Felice G, Gobbin F, Roselli I, Sangirardi M, et al. Low-impact techniques for seismic strengthening fair faced masonry walls. Constr Build Mater 2021;307:124962. https://doi.org/10.1016/j.conbuildmat.2021.124962.
[55] Prota A, Zito M, D'Angela D, Toscano G, Ceraldi C, Fiorillo A, et al. Preliminary results of shake table tests of a typical museum display case containing an art object. Adv Civ Eng 2022;2022:1–18. https://doi.org/10.1155/2022/3975958.
[56] Verderame GM, Balsamo A, Ricci P, Di Domenico M, Maddaloni G. Experimental assessment of the out-of-plane response of strengthened one-way spanning masonry infill walls. Compos Struct 2019;230:111503. https://doi.org/10.1016/j.compstruct.2019.111503.
[57] Petrone C, Magliulo G, Manfredi G. Shake table tests on standard and innovative temporary partition walls. Earthq Eng Struct Dyn 2017;46:1599–624. https://doi.org/10.1002/eqe.2872.
[58] Zou X, Yang W, Wang M, Liu P. Seismic effectiveness assessment of nylon lines for the protection of museum artifacts via shaking table tests. Constr Build Mater 2024;418:135340. https://doi.org/10.1016/j.conbuildmat.2024.135340.
[59] Chopra A.K. Dynamics of structures: theory and applications to earthquake engineering. 3rd ed. Upper Saddle River, N.J: Pearson/Prentice Hall; 2007.
[60] Arlinghaus S. Practical Handbook of Curve Fitting. 1st ed. Boca Raton: CRC Press; 2023. https://doi.org/10.1201/9781003418221.
[61] Roselli I, Fioriti V, Canio GD. Use of the transmissibility function H for ambient vibration measurements of an archeological building. Metrol. Archaeol. Cult. Herit. MetroArchaeo, Cassino FR, 2018. Italy: IEEE; 2018. p. 390–5. https://doi.org/10.1109/MetroArchaeo43810.2018.9089806.
[62] Butterworth J., Lee J.H., Davidson B. Experimental determination of modal damping from full scale testing. Proc. 13th World Conf. Earthq. Eng., Vancouver, British Columbia, Canada: 2004, p. 1–15.
[63] Filiatrault A, Perrone D, Merino RJ, Calvi GM. Performance-based seismic design of nonstructural building elements. J Earthq Eng 2018:1–33. https://doi.org/10.1080/13632469.2018.1512910.
[64] Anajafi H, Medina RA. Evaluation of ASCE 7 equations for designing acceleration-sensitive nonstructural components using data from instrumented buildings. Earthq Eng Struct Dyn 2018;47:1075–94. https://doi.org/10.1002/eqe.3006.
[65] Zhong Z, Guo Q, Shen J, Zhao M, Du X. Shaking table tests and out-of-plane seismic performance assessment of lightweight hollow partition walls. Eng Struct 2025;342:120968. https://doi.org/10.1016/j.engstruct.2025.120968.
[66] Berto L, Sarno LD, Rocca I. Seismic isolation of museum artefacts: experimental validation through shake table tests. Earthq Eng Struct Dyn 2025. https://doi.org/10.1002/eqe.70005.
[67] American Society of Civil Engineers. Minimum Design Loads and Associated Criteria for Buildings and Other Structures. 7th ed. Reston, VA: American Society of Civil Engineers; 2017. https://doi.org/10.1061/9780784414248.
[68] International Organization for Standardization (ISO). BS ISO 13033:2013. Bases for design of structures. Loads, forces and other actions. Seismic actions on nonstructural components for building applications. 60.60. 2013.
[69] Preti M, Migliorati L, Giuriani E. Experimental testing of engineered masonry infill walls for post-earthquake structural damage control. Bull Earthq Eng 2015;13:2029–49. https://doi.org/10.1007/s10518-014-9701-2.
[70] Pantò B, Rossi PP. A new macromodel for the assessment of the seismic response of infilled RC frames. Earthq Eng Struct Dyn 2019;48:792–817. https://doi.org/10.1002/eqe.3163.
[71] Mohamed H, Romão X. Analysis of the performance of strut models to simulate the seismic behaviour of masonry infills in partially infilled RC frames. Eng Struct 2020;222:111124. https://doi.org/10.1016/j.engstruct.2020.111124.
[72] Applied Technology Council, Federal Emergency Management Agency, Project team. FEMA P-58-1. Seismic performance assessment of buildings, Volume 1, Methodology. 2018.
[73] Moehle J., Deierlein G.G. A FRAMEWORK METHODOLOGY FOR PERFORMANCE-BASED EARTHQUAKE ENGINEERING. Proc. 13th World Conf. Earthq. Eng., Vancouver, B.C., Canada: 2004, p. Paper No. 679.
[74] D'Angela D, Magliulo G. Methodological guidance and quantitative measures regarding seismic capacity and safety of freestanding and inelastic anchored nonstructural elements housed in ordinary and critical facilities. Reliab Eng Syst Saf 2025;260:111029. https://doi.org/10.1016/j.ress.2025.111029.
[75] ATC-58 Nonstructural Performance Products Team. ATC-58 Project Task Report Phase 2, Task 2.3 Engineering Demand Parameters for Nonstructural Components. 201 Redwood Shores Parkway, Suite 240 Redwood City, California 94065: APPLIED TECHNOLOGY COUNCIL; 2004.
[76] Jenkins C, Soroushian S, Rahmanishamsi E, Maragakis EM. Experimental fragility analysis of cold-formed steel-framed partition wall systems. ThinWalled Struct 2016;103:115–27. https://doi.org/10.1016/j.tws.2016.02.015.

[77] British Standards Institution, European Committee for Standardization. Eurocode 8, design of structures for earthquake resistance. London: British Standards Institution; 2005.
[78] American Society of Civil Engineers. Minimum Design Loads and Associated Criteria for Buildings and Other Structures. Reston, VA: American Society of Civil Engineers; 2021. https://doi.org/10.1061/9780784415788.
[79] Ministero delle Infrastrutture e dei Trasporti. Circolare 21 gennaio 2019, n. 7C.S. LL.PP. Istruzioni per l'applicazione dell'«Aggiornamento delle "Norme tecniche per le costruzioni"» di cui al decreto ministeriale 17 gennaio 2018 (in Italian) 2019.
[80] Dhakal RP, Pourali A, Saha SK. Simplified seismic loss functions for suspended ceilings and drywall partitions. Bull N Z Soc Earthq Eng 2016;49:64–78. https://doi.org/10.5459/bnzsee.49.1.64-78.
[81] Ricci P, Manfredi V, Noto F, Terrenzi M, Petrone C, Celano F, et al. Modeling and seismic response analysis of Italian code-conforming reinforced concrete buildings. J Earthq Eng 2018;22:105–39. https://doi.org/10.1080/13632469.2018.1527733.
[82] Ministero del Lavoro e delle Politiche Sociali. Decreto direttoriale n. 12 del 5.4.2023 (in Italian). 2023.